FasR regulates fatty acid biosynthesis and is essential for virulence of *Mycobacterium tuberculosis*

Sonia Mondino[a,*], Cristina Lourdes Vázquez[b], Matías Cabruja[a,*], Claudia Sala[c,*], Amaury Cazenave-Gassiot[d], Federico Carlos Blanco[b], Markus R. Wenk[d], Fabiana Bigi[b], Stewart T. Cole[c,*], Hugo Gramajo[a] and Gabriela Gago[a#]

[a] Laboratory of Physiology and Genetics of Actinomycetes, Instituto de Biología Molecular y Celular de Rosario (IBR-CONICET), Facultad de Ciencias Bioquímicas y Farmacéuticas, Universidad Nacional de Rosario, Argentina
[b] Instituto de Biotecnología-IABIMO, UEDD CONICET-Instituto Nacional de Tecnología Agropecuaria (INTA), Argentina.
[c] Global Health Institute, Ecole Polytechnique Fédérale de Lausanne, Lausanne, Switzerland.
[d] Singapore Lipidomics Incubator (SLING), Life Sciences Institute, and Department of Biochemistry, Yong Loo Lin School of Medicine, National University of Singapore, Singapore.

Running Head: FasR is essential for *M. tuberculosis* virulence

Address correspondence to Gabriela Gago, gago@ibr-conicet.gov.ar

[*] Sonia Mondino and Stewart T. Cole present address: Institut Pasteur, Paris (France)

[*] Matías Cabruja present address: Stanford University (United States)

[*] Claudia Sala present address: Fondazione Toscana Life Sciences, Siena (Italy)

Sonia Mondino, Cristina L. Vázquez and Matías Cabruja contributed equally to this work. Author order was determined on the basis of contributions.

The abstract has 247 words and the text has 5215 words (including Materials and Methods).

Abstract

Mycobacterium tuberculosis, the etiologic agent of human tuberculosis, is the world's leading cause of death from an infectious disease. One of the main features of this pathogen is the complex and dynamic lipid composition of the cell envelope, which adapts to the variable host environment and defines the fate of infection by actively interacting with and modulating immune responses. However, while much has been learned about the enzymes of the numerous lipid pathways, little knowledge is available regarding the proteins and metabolic signals regulating lipid metabolism during *M. tuberculosis* infection. Previous studies identified FasR as an essential transcriptional activator of *de novo* fatty acid biosynthesis in *Mycobacterium smegmatis*. In this work, we constructed and characterized a FasR-deficient mutant in *M. tuberculosis* and demonstrated that FasR positively regulates *fas* and *acpS* expression. Lipidomic analysis of the wild type and mutant strains revealed complete rearrangement of most lipid components of the cell envelope, with phospholipids, mycolic acids, sulfolipids and phthiocerol dimycocerosates relative abundance severely altered. As a consequence, replication of the mutant strain was impaired in macrophages leading to reduced virulence in a mouse model of infection. Moreover, we show that the *fasR* mutant resides in acidified cellular compartments, suggesting that the lipid perturbation caused by the mutation prevented *M. tuberculosis* inhibition of phagolysosome maturation. This study identified FasR as a novel factor involved in regulation of

mycobacterial virulence and provides evidence for the essential role that modulation of lipid homeostasis plays in the outcome of *M. tuberculosis* infection.

Importance

Tuberculosis is the leading cause of death from a single infectious disease, resulting in approximately 1.5 million deaths per year worldwide. The composition and complexity of the cell envelope is the most distinctive feature of *Mycobacterium tuberculosis*, the etiologic agent of human tuberculosis. As the mycobacterial cell envelope is the interface with the host, the modulation of its structure and consequent responsiveness to immune factors might be important in determining the state of an infection. In this study, a *M. tuberculosis* mutant strain in FasR was constructed and analyzed. Inactivation of *fasR* in *M. tuberculosis* was not lethal for *in vitro* growth but led to rearrangement of the lipid composition of the cell envelope. Consequently, the mutant strain was less virulent in a mouse model of infection and showed impaired replication in macrophages, thus implying that lipid homeostasis plays an important role during *M. tuberculosis* infection.

Introduction

Tuberculosis (TB) is one of the top ten causes of death and the leading cause from a single infectious agent, exceeding both malaria and HIV. In 2018, there were an estimated 10 million new cases of active TB and 1.3 million patients died from active infection (1). The emergence of multidrug-resistant TB (MDR-TB) presents

an increasingly difficult therapeutic challenge; consequently, MDR-TB is now the main cause of death due to antimicrobial resistance (1) thus transforming this long neglected disease into a global health priority.

The composition and complexity of the cell envelope is the most distinctive feature of *Mycobacterium tuberculosis*, the etiologic agent of human TB. Biochemical and microscopic data revealed that the mycobacterial envelope consists of three discrete entities: a plasma membrane surrounded by a complex cell wall and an outermost layer called the capsule in pathogenic species (2, 3). The *M. tuberculosis* cell wall consists of peptidoglycan covalently linked to arabinogalactan esterified by mycolic acids (MA), which form the inner leaflet of the outer membrane bilayer (mycomembrane). The outer leaflet of this membrane is composed of free, non-covalently bound lipids and glycolipids like trehalose monomycolates (TMM), trehalose dimycolates (TDM), glycerol monomycolates, glucose monomycolates, phthiocerol dimycocerosates (PDIM), poly acylated trehaloses (PAT), sulfolipids (SL), phosphatidylinositol mannosides (PIM), phenolic glycolipids (PGL) and mannose-capped lipoarabinomannans (Man-Lam) (4, 5).

During the course of infection, intracellular pathogenic bacteria use different strategies to survive, multiply and persist inside the host (6). *M. tuberculosis* encounters heterogeneous host environments, including high oxygen tension in the lung alveolus, reactive oxygen and nitrogen species in activated macrophages, as well as nutrient depletion and hypoxia in tuberculous granulomas. How *M. tuberculosis* survives these diverse environments is not fully understood. *M. tuberculosis* has evolved a wide array of specific lipids and related metabolic pathways that actively interact with the immune system, and multiple reports from

human and animal studies suggest an intimate link between *M. tuberculosis* lipid metabolism and outcome of infection (7–9). Of particular interest is the challenge that *M. tuberculosis* must face in order to adjust its own lipid metabolism while the macrophage is changing its lipid content (10). Little is known about the mechanism underlying the reorganization of *M. tuberculosis* envelope during infection (11). Understanding how this pathogen selects and organizes the envelope components to resist killing, and how these components make the envelope essential to *M. tuberculosis* survival, virulence and pathogenesis, is still a major challenge. Therefore, characterization of the regulatory elements that control these processes should help improve understanding of the mechanisms involved in mycobacterial pathogenicity and could provide new potential targets for anti-TB chemotherapy.

Previous studies on the regulation of lipid biosynthesis in mycobacteria allowed us to identify FasR as the transcriptional activator of fatty acid biosynthesis in *M. smegmatis* (12). Deletion of *fasR* from *M. smegmatis* was possible only in the presence of an extra copy of the gene, suggesting that *fasR* is essential for viability. Notably, we found that the affinity of FasR for its target promoter is modulated by long chain acyl-CoAs ($\geq C_{16}$), the end products of the FAS I pathway. FasR, together with MabR, the transcriptional regulator of MA biosynthesis, are the only transcription factors involved in fatty acid biosynthesis regulation known to be essential for *M. smegmatis* survival, reflecting the relevance of lipid homeostasis for mycobacterial viability (12, 13).

In this study, a *M. tuberculosis* knockout strain in *fasR* was constructed and the mutant used to analyze the implications of lipid homeostasis in *M. tuberculosis* virulence. Inactivation of *fasR* in *M*. *tuberculosis* was not lethal for *in vitro* growth

but led to complete rearrangement of lipid composition of the envelope. Consequently, the mutant strain was less virulent in a mouse model and showed impaired replication in macrophages, thus implying that lipid homeostasis plays an important role during *M. tuberculosis* infection.

Results

Construction and characterization of *M. tuberculosis fasR* mutant strain

To investigate the function of FasR in *M. tuberculosis,* and considering that *fasR* is essential for *M. smegmatis* viability, we first constructed an *M. tuberculosis* conditional knockdown strain in *fasR* (Fig 1A-B). Plasmids pFR33, providing a second copy of *fasR* under the control of the TET-PIP OFF system at the chromosomal L5 phage attachment site *attB* (14) and pGA80, were simultaneously transformed in *M. tuberculosis* (Table S1). Disruption of *fasR* was then obtained by two-step allelic exchange using pFR35, which deleted the gene at the native locus. Homologous recombination was confirmed by colony PCR and Southern blot analysis, and the resulting conditional knockdown strain was named *Mtb*Δ*fasR*-c*fasR* (Fig 1D). In this strain, expression of *fasR* was downregulated by addition of anhydrotetracycline (ATc) to the culture medium, thus leading to protein depletion. However, we were not able to detect any growth defect after addition of ATc, suggesting that *fasR* was not essential for *M. tuberculosis* survival. This result prompted us to try to obtain a *fasR* knockout (KO) mutant strain by replacing the *fasR* complementing plasmid with the empty vector pND255 (Fig 1C). Consistent

with the ability of the conditional mutant to grow in the non-permissive condition, plenty of colonies were obtained in the presence of Hyg, and the replacement was successfully confirmed by colony PCR (Fig S1A). We selected two Hyg-resistant clones and confirmed the depletion of FasR by Western blot using total protein extracts (Fig S1B). The genotype of this strain was further analyzed by Southern Blot (Fig 1D), thus validating the genomic deletion of *fasR* and the generation of the *fasR* KO mutant strain, named *Mtb*Δ*fasR*.

Once the non-essentiality of *fasR* for *M. tuberculosis* survival was confirmed, we then hypothesized that deletion of this transcriptional regulator could be deleterious for bacterial growth under specific conditions. In particular, we analyzed the growth of *Mtb*Δ*fasR* mutant using different culture media. As shown in Fig 2, growth of *Mtb*Δ*fasR* in complete 7H9 medium (7H9 + OADC) was similar to that of the wild type and the complemented strain (*Mtb*Δ*fasR*-c*fasR* grown without ATc), although the KO mutant reached stationary phase earlier and at lower OD_{600}. Interestingly, if the medium was not supplemented with oleate and BSA (i.e. 7H9 without OADC), growth defects appeared to be more pronounced, suggesting that the presence of lipids in complete 7H9 medium could partially rescue the absence of FasR. Moreover, *Mtb*Δ*fasR* mutant showed severe growth defects in Sauton minimal medium, reaching a maximal OD_{600} of 0.3 (Fig 2). Altogether, these experiments showed that FasR is not essential for *M. tuberculosis* survival, although it is required for optimal bacterial growth, especially under lipid-limited conditions.

FasR is a transcriptional activator of the *fas-acpS* operon in *M. tuberculosis*

We have previously demonstrated that FasR is a transcriptional activator of *fas* in *M. smegmatis* (12). Thus, to validate the role of FasR in fatty acid biosynthesis in *M. tuberculosis*, we analyzed expression of the *fas-acpS* operon genes in *Mtb*Δ*fasR* and in the complemented strain *Mtb*Δ*fasR*-c*fasR*. The relative amounts of *fas* and *acpS* mRNAs were measured by quantitative RT-PCR after 8 days of growth in complete 7H9 medium and compared to those of *Mtb*H37Rv wild type strain. As shown in Fig 3, transcription of *fas* and *acpS* was reduced by 70 % and 40 % respectively when cells were deprived of FasR, confirming that FasR is a transcriptional activator of the *fas-acpS* operon in *M. tuberculosis*.

fasR knockout strongly impacts composition of _M. tuberculosis_ cell envelope

Previous characterization of *M. smegmatis fasR* (12) and *fas* (15) conditional mutant strains revealed that reduced FAS I levels had a strong impact on fatty acid and phospholipid biosynthesis. Interestingly, MA remained being synthesized in the FAS I mutant for several hours after addition of ATc (non-permissive conditions), although with different abundance of the various species (15). Considering the relevance that lipids have in *M. tuberculosis* survival and virulence, the impact of the absence of FasR on the global lipid profile of *M. tuberculosis* was further studied. We performed comparative lipidomic analyses between *Mtb*H37Rv, *Mtb*Δ*fasR* and the complemented strain. Briefly, we extracted cell-associated lipids as previously described (15) and analyzed the lipid content by high-performance liquid chromatography-mass spectrometry with data-dependent tandem MS (HPLC-MS/MS).

As illustrated in Fig 4, lipid analysis in the negative mode indicated that the relative abundance (expressed as percentage of lipid MS signals) of phospholipids (PL) and MA in the wild type and complemented strains was approximately 75 and 25 %, respectively. These values changed to 50 % for both PL and MA in the *fasR* mutant strain, reflecting the strong impact that lower levels of *de novo* fatty acid biosynthesis had in PL and MA relative abundance. The relative composition of PL also showed a biased effect towards phosphatidylinositol (PI) and cardiolipins (CL), which were significantly reduced in the mutant strain (Figs 4 and S2). Furthermore, there was a strong reduction in the content of sulfolipids (Figs 4 and S2) and the acyl chain substitutions of this lipid were consistently shorter in the mutant strain (Fig S3). A relevant change observed in the qualitative composition of the PL was the significant increase in the double bonds of the acyl residues in the mutant strain, with those of the CL, phosphatidylglycerol (PG) and PI being most significant (Fig S4).

Additionally, results obtained in the positive mode analysis showed that *M. tuberculosis MtbΔfasR* mutant strain displayed a significant reduction in the relative content of PDIM (Figs 5 and S2), with acyl substitutions that are shorter in the mutant strain, compared with the wild type or the complemented strain (Fig S3). Most of the changes observed in the deletion mutant were reversed in the complemented strain *MtbΔfasR-cfasR*, indicating that *fasR* is needed to maintain the global lipid composition of *M. tuberculosis* cell envelope.

FasR is required for *M. tuberculosis* replication in macrophages

To investigate whether FasR is required for the intracellular survival of *M. tuberculosis* in macrophages, we infected THP-1-derived macrophages with exponentially growing cultures of *Mtb*H37Rv, *Mtb*Δ*fasR* and the complemented strain *Mtb*Δ*fasR*-c*fasR*. To quantify bacterial uptake and intracellular replication, we determined the numbers of intracellular viable bacteria at different time points post-infection. As shown in Fig 6, infection with similar numbers of bacteria of each strain resulted in recovery of similar numbers of CFU for all of the strains at 24 and 48 h post-infection. However, 120 and 144 h after the infection, intracellular bacterial replication of *Mtb*Δ*fasR* strain was significantly reduced compared to that of the wild type strain. The wild type phenotype was partially restored in the *Mtb*Δ*fasR*-c*fasR* complemented strain at day 5 (120 h) and completely restored at day 6 (144 h), indicating that the intracellular growth defect was due to the deletion of *fasR* and that this regulator is necessary for optimal intracellular multiplication of *M. tuberculosis* in macrophages.

FasR regulates phagosome maturation in macrophages

We have shown that the absence of FasR, and consequently reduced levels of *fas-acpS*, have a strong impact on the composition of *M. tuberculosis* cell envelope, and also on bacterial multiplication within macrophages. We hypothesized that the altered bacterial cell envelope of the *Mtb*Δ*fasR* mutant may affect *M. tuberculosis*-driven phagosome maturation during infection. To investigate this, we analyzed the acidification of *M. tuberculosis Mtb*Δ*fasR* phagosome during infection of human macrophages by staining with Lysotracker dye and measuring the phagosomal acquisition of LAMP-3 (late endosomal/lysosomal markers). Interestingly, while

*Mtb*H37Rv prevented phagosome acidification, *Mtb*Δ*fasR* mutant strain resided in phagosomes that were strongly stained by Lysotracker dye and that acquired LAMP-3, suggesting that this strain cannot avoid phagosomal maturation. The observed mutant phenotype was rescued in the *Mtb*Δ*fasR*-c*fasR* complemented strain, indicating that the increased phagosome acidification was due to the absence of FasR (Fig 7).

Disruption of lipid homeostasis attenuates mycobacterial virulence in mice

To characterize the role of FasR in an experimental model of infection, three groups of BALB/c mice (10 per group) were infected intratracheally with 10^2 CFU of *Mtb*H37Rv, *Mtb*Δ*fasR* and *Mtb*Δ*fasR*-c*fasR* strains. Mice were killed 60 days post-infection and bacterial loads in lungs were determined. CFU counts were significantly reduced for the *Mtb*Δ*fasR* strain compared to *Mtb*H37Rv, while the wild type phenotype was restored in the *Mtb*Δ*fasR*-c*fasR* strain (Fig 8), indicating that FasR is essential for survival and multiplication of *M. tuberculosis* in mice.

Discussion

In a previous investigation we identified FasR, a TetR-like transcriptional regulator that specifically binds to the *fas* promoter region to activate its expression, and found that FasR was essential for *in vitro* growth of *M. smegmatis* (12). However, its role in *M. tuberculosis* viability was controversial. Using Himar 1 transposon mutagenesis it was initially proposed that FasR was essential for *M. tuberculosis*

survival (16, 17). However, more recently, De Jesus *et al* found that FasR was dispensable for growth, by assessing the composition of a highly saturated library of transposon mutants *of M. tuberculosis* by deep sequencing (18). Moreover, the relevance of FasR for mycobacterial survival in intracellular environments or animal models had not been investigated. In this work, by constructing a deletion *fasR* mutant and a complemented strain, we unequivocally established that FasR is not essential for *M. tuberculosis* viability, although it is required for optimal growth of *M. tuberculosis in vitro* and for virulence in macrophages and mice model of infection.

We had shown that FasR binds to three inverted repeats present in the promoter region of the *fas-acpS* operon thereby activating fatty acid biosynthesis in *M. smegmatis* (12). Furthermore, we also demonstrated, *in vitro* and *in vivo,* that FasR binding to its target promoter is regulated by long-chain acyl-CoAs, the main products of FAS I (12). The *fas* and *acpS* genes form a bicistronic operon, coding for the FAS I synthase and the 4-phosphopantetheinyl transferase, respectively; the latter being an essential enzyme to produce functional acyl carrier protein (holo ACP), central to all fatty-acid biosynthesis systems. Transcriptional studies carried out in this work showed that expression of the *fas-acpS* operon genes in *M. tuberculosis* Δ*fasR* was reduced by 70 % and 40 %, respectively (Fig 3). This result confirmed that FasR is a transcriptional activator of the *fas-acpS* operon in *M. tuberculosis*. The activator nature of FasR highlights a remarkable difference with most transcriptional regulators of fatty acid biosynthesis, which are repressor proteins (19). Moreover, FasR is a member of the TetR family of regulators, and the vast majority of these proteins are transcriptional repressors, with very few acting as activators (20).

Since fatty acids are major constituents not only of phospholipids but also of several complex lipids, inactivation of FasR was expected to modify synthesis of several components of the cell envelope essential for mycobacterial viability and/or virulence. Indeed, lipidomic analysis of *Mtb*Δ*fasR* and comparison with wild type and complemented strains proved this hypothesis. As expected, reduced levels of fatty acid biosynthesis in *Mtb*Δ*fasR* had a strong impact on relative abundance of phospholipids and their relative and qualitative composition (Figs 4 and S2). Phosphatidylinositol (PI) and cardiolipins (CL) were significantly reduced in the mutant strain, while the acyl chains present in and these phospholipids exhibited a significant increase in their double bond content (Fig S4). Mycobacterial phospholipids have been implicated in immunomodulation. For example, CL is processed into lysocardiolipin by the lysosomal phospholipase A2 during infection, probably generating active lipid derivatives that play important roles during infection or persistence within the host (21). The *Mtb*Δ*fasR* mutant strain also displayed a strong reduction in the content of sulfolipids (Figs 4 and S2) and PDIM (Figs 5 and S2). Interestingly, the acyl chain substitutions of both lipids were consistently shorter compared to the wild type *Mtb*H37Rv strain (Fig S3). On this regard, a *M. tuberculosis* mutant strain deficient in sulfolipids and PDIM has been shown to be attenuated in macrophages and in mice models of infection (8). Moreover, during infection, genes involved in the biosynthesis of sulfolipids and PDIM are upregulated (22, 23) and the mass of these lipids increases (24, 25). Altogether, our results showed that *M. tuberculosis fasR* mutant exhibits an extensive rearrangement of the lipid components of the cell envelope, that are reversed in the complemented strain *Mtb*Δ*fasR*-c*fasR*, confirming that FasR is

needed to maintain the lipid homeostasis of the *M. tuberculosis* cell envelope. As the mycobacterial cell envelope is the interface with the host, FasR modulation of its structure and consequent responsiveness to immune factors might be important in determining the state of an infection.

Consistent with this hypothesis, we have shown that FasR is necessary for optimal intracellular multiplication of *M. tuberculosis* in macrophages, therefore confirming the role of cell wall components in the ability of the pathogen to survive and multiply intracellularly (26). Persistence of the tubercle bacillus inside cells relies upon inhibition of phagosome maturation and acidification (27). In this context, several cell wall lipids have been shown to modulate host endocytic pathways. This is the case for Man-Lam, TDM, PIM and PDIM, which, besides their role in phagocytosis, also mediate intracellular trafficking and vacuole maturation arrest induced by *M. tuberculosis* (8). More recently, PDIM and SL were shown to be involved in controlling autophagy-related pathways in human macrophages (28). Considering the changes observed in the PDIM content of the *Mtb*Δ*fasR* mutant, we analyzed the acidification of phagosome during infection of human macrophages. Interestingly, while the wild type *Mtb*H37Rv and the complemented strains prevented phagosome acidification, the *Mtb*Δ*fasR* mutant was impaired in avoiding phagosomal maturation, clearly indicating that increased phagosome acidification was due to absence of FasR (Fig 7). These results suggested that although FasR is not essential for *in vitro* growth, regulation of lipid biosynthesis, mediated by FasR, is critical for macrophage infection. Moreover, using a mouse model of infection we demonstrated the essentiality of FasR for *M. tuberculosis*

virulence *in vivo* (Fig 8), most probably as a consequence of the loss of various mycobacterial lipids that contribute to pathogenicity.

Co-evolution with the human immune system prompted *M. tuberculosis* to generate exquisite mechanisms of immunomodulation and immune evasion, many of which depend on its cell envelope. In fact, comparison of cell envelope components between *M. tuberculosis* and ancestral species revealed a restructuring of the mycomembrane glycolipid components, including mycolic acids and free lipids of the outer leaflet (11). The observed phenotype of the FasR mutant is probably a consequence of additive effects, as several components of the cell envelope were altered. *M. tuberculosis* interferes with innate immune signalling pathways, for example by masking pathogen-associated molecular patterns with PDIM (29) and inhibiting toll-like receptor 2 with sulfoglycolipids (30). PDIM is also crucial for other steps of infection: it contributes to cell envelope properties, such as the permeability barrier (31), improves the invasiveness of *M. tuberculosis* and its capacity to arrest phagosome maturation, possibly by inducing changes in the plasma membranes of human macrophages during infection (32), and directly protects against reactive nitrogen species (33). Therefore, reduced content of these molecules (and/or changes in their chemical composition) may contribute to sensitivity to the bactericidal activities of phagocytes.

Altogether, our data indicate an important role for FasR in *M. tuberculosis* pathogenesis and encourage further investigations into the contribution of lipid regulation to virulence. It is well known that *M. tuberculosis* is able to modulate the expression of its cell wall components in response to environmental changes, however, little is known about their reorganization during infection, and to a lesser

extent about the regulatory mechanisms involved in this process (11). The dynamism of the bacterial cell envelope should be a tightly regulated phenomenon, ensuring *M. tuberculosis* survival during infection. Thus, specific regulatory components involved in this process, as we have demonstrated for FasR, would constitute interesting targets for the development of new treatment strategies.

Along this line of thinking, we recently solved the crystal structures of *M. tuberculosis* FasR in complex with DNA and the acyl effector ligands, which provided insights into the molecular sensory and transmission mechanisms of this regulatory protein (34). This knowledge could lead now to perform structure-guided drug discovery strategies to identify anti-mycobacterial molecules with novel mechanisms of action.

Materials and methods

Ethics statement

All animal experiments were performed in compliance with the regulations of the Institutional Animal Care and Use Committee (CICUAE) of INTA with the authorization Number 20/2016.

Bacterial strains, culture and transformation conditions

The *E. coli* strain DH5α (35) was used for routine subcloning and was transformed according to Sambrook *et al.* (36). *M. tuberculosis* H37Rv (37), *Mtb*Δ*fasR* and *Mtb*Δ*fasR*-c*fasR* were grown at 37 ºC in Middlebrook 7H9 broth supplemented with

0.2 % glycerol, 0.03 % Tyloxapol and 10 % OADC or Middlebrook 7H10 agar supplemented with 0.2 % glycerol and 10 % OADC. Hygromycin (Hyg, 50 µg/ml), kanamycin (Kan, 15 µg/ml) and streptomycin (Str, 12 µg/ml) were added when needed.

Recombinant plasmids and strain genotypes are listed in electronic supplementary material (Tables S1 and S2).

DNA manipulation, plasmid construction and mutant generation

Genomic DNA of *M. tuberculosis* was obtained as described previously (38). For the construction of the *fasR* mutant allele, a fragment of 946 bp containing 58 bp of the *fasR* 5´end plus 882 bp of the upstream region was PCR amplified from genomic DNA using oligonucleotides 3208_1up and 3208_2down (Table S3). The PCR product was cloned in the pCR BluntII TOPO vector (Invitrogen). The resulting plasmid was digested first with *Eco*RV and after with *Xho*I/*Nde*I. The 940 bp fragment obtained was cloned in the suicide vector pJG1100 (39, 40) digested with the same enzymes, generating plasmid pFR34. Additionally, a fragment of 883 bp containing 87 bp of the *fasR* 3´end plus 784 bp of the downstream region was PCR amplified from genomic DNA using oligonucleotides 3208_3up and 3208_4down (Table S3). The PCR product was cloned in the pCR BluntII TOPO vector (Invitrogen). The resulting plasmid was digested first with *Eco*RI and after with *Nde*I/*Spe*I and the fragment (877 bp) was cloned in pFR34 vector digested with the same enzymes, generating plasmid pFR35.

For the construction of a *fasR* merodiploid strain, the fragment resulting from the digestion of the plasmid pFR3 (12) with *Xba*I and *Eco*RI was cloned between the *Avr*II and *Mfe*I sites in plasmid pGA44 (41). The resulting plasmid, pFR33, is an integrative plasmid that harbours *fasR* expressed under the control of *Ptr* promoter and the TetR/Pip OFF system necessary for its regulation.

Deletion of *fasR* was accomplished by homologous recombination. After transformation of *M. tuberculosis* with plasmid pFR35, the first recombination event was selected on 7H10 medium containing Kan and Hyg and resistant colonies were screened by colony PCR. The merodiploid strain was generated by integration of pFR33 at the L5 *attB* site and transformants were plated on 7H10 with Hyg, Kan and Str. Deletion of the wild type gene by allelic replacement was accomplished by plating bacteria on 7H10 agar plates supplemented with Str and 2.5 % sucrose. The Hyg^s, Kan^s, Str^r, $Sucrose^r$ colonies were tested by PCR and the *fasR* conditional knockdown strain was named *Mtb*Δ*fasR*-c*fasR*. Generation of a *fasR* knockout strain (*Mtb*Δ*fasR*) was obtained by swapping the pFR33 plasmid at the L5 *attB* site with the pND255 plasmid. Transformants were selected on 7H10 plates containing Hyg. Deletion of *fasR* was confirmed by Southern Blot and colony PCR.

Southern Blot

10 µg of genomic *M. tuberculosis* DNA was digested overnight with an excess of *Xho*I, and the fragments were separated by electrophoresis in a 0.7% agarose gel. Southern blotting was carried out using Hybond-N^+ membrane (Amersham) and DIG High Prime DNA Labeling and Detection Starter kit II (Roche), following the indications of the manufacturer. The probe consisted of a 594 bp fragment

amplified with oligonucleotides Southern_1fasRTB and Southern_2fasRTB (Table S3), corresponding to the upstream genomic region of *fasR*.

Western blot

Equal amounts of protein extracts were loaded on 4-12 % NuPAGE gels (Invitrogen) and transferred onto nitrocellulose membranes using a dry electrophoresis transfer apparatus (Invitrogen). Membranes were incubated in TBS-Tween blocking buffer (20 mM Tris pH 7.5, 150 mM NaCl, 0.1 % Tween 20) with 5 % (w/v) skimmed milk powder for 2 h at 4 ºC prior to overnight incubation with 1:1000 dilution of monoclonal anti-FasR primary antibody (Alere^{TM}). Membranes were washed in TBS-Tween three times at room temperature, and then incubated with 1:100000 secondary antibody Anti-Mouse Kappa conjugated to Horseradish Peroxidase (Southern Biotech) for 2 h before washing again. Signals were detected using Chemiluminescent Peroxidase Substrate (Sigma-Aldrich). Monoclonal mouse anti-RpoB antibodies were purchased from NeoClone and used 1:20000.

RNA techniques

RNA was extracted from *M. tuberculosis* strains grown for 8 days in complete 7H9 media using Trizol-phenol based methods (41) and treated, when needed, with RQ1 RNase-Free DNase (Promega). qRT-PCR was performed using second strand cDNA as the template, generated with SuperScript III Reverse Transcriptase (Invitrogen), random primers and a green fluorochrome as the indicator dye (qPCR master mix, Biodynamics). The expression of *fas*, *fasR* and *acpS* was quantified after normalization of RNA levels to the expression of the *sigA*

gene as previously described (15). qPCR data are presented as relative expression values normalized to *sigA* and to the wild type strain H37Rv. qPCR cycling conditions were as follows: 95 ºC for 2 min followed by 40 cycles of 95 ºC for 15 s, 58 ºC for 15 s and 68 ºC for 20 s. The sequences of all the primers used are listed in electronic supplementary material (Table S3).

Lipid analysis

Cell-associated lipid for lipidomic analyses were prepared as previously described (15). Briefly, cell pellets of cultures grown at 37 ºC in Middlebrook 7H9 broth (DIFCO) supplemented with 0.2 % glycerol, 0.03 % Tyloxapol and 10 % OADC were washed with 50 mM ammonium acetate, pH 7.8 and transferred to glass tubes containing 5 ml $CHCl_3$:CH_3OH (2:1, v/v). Samples were incubated overnight at 4 ºC with gentle agitation. After centrifugation, bacterial pellets were subjected to an additional extraction using $CHCl_3$:CH_3OH (1:2, v/v) for 2 h. Organic extracts were pooled and dried under nitrogen at 4 ºC. Lipids were resuspended in 3 ml of $CHCl_3$, washed with 3 ml of H_2O and the organic phase was transferred to pre-weighted glass tubes, dried under nitrogen at 4 ºC and re-weighted on a microbalance. Extracts were dissolved in $CHCl_3$:CH_3OH (1:1, v/v) at 1 mg ml^{-1} and centrifuged at 3000 g for 5 min. Lipids were analyzed in an Agilent 1200 series HPLC system with a Reprospher (Dr Maish) 100 C8 column (1.8 µm, 50 mm length, 2 mm ID). The flow rate was 0.3 ml min^{-1} in binary gradient mode with the following elution program: the column was equilibrated with 100 % mobile phase A [CH_3OH:H_2O (99:1, v/v), containing 0.05 mM $AcNH_4$]. 2 µl of each sample were

injected, and the same elution conditions continued for 1 min, followed by a 12 min gradient to 100 % mobile phase B [isopropanol:hexane:H_2O (79:20:1, v/v), containing 0.05 mM $AcNH_4$], finally holding this condition for 1 min. The column was equilibrated for 2 min with 100 % mobile phase A before injection of the next sample. An Agilent 6500 series Q-TOF instrument with a Dual AJS ESI was used for mass analysis. Ionization gas temperature was maintained at 200 ºC with a 14 l min^{-1} drying gas flow, a 35 psig nebulizer pressure and 3500 Volts. Spectra were collected in positive and negative mode from *m/z* 115 to 3000 at 4 spectra s^{-1}. Automatic tandem-MS (MS-MS) was obtained in data-dependent acquisition mode at 15 MS-MS per cycle. Continuous infusion calibrants included *m/z* 121.051 and 922.010 in positive-ion mode and *m/z* 119.035 and 955.972 in negative-ion mode. CID-MS was carried out with an energy of 50 volts. For the comparative analysis, the column is conditioned by four successive mock injections before randomized QCs and mycobacterial samples are analyzed. Lipid features were annotated based on structural MS-MS information. Lipid classes' retention times (RT) were identified using characteristics fragmentation patterns (42). Individual molecules in each class were then identified based on exact mass and RT.

Colony-forming units (CFU) analysis

M. tuberculosis H37Rv, *Mtb*Δ*fasR* and *Mtb*Δ*fasR*-c*fasR* strains were used to infect THP-1 cells (MOI=5). The day before infection $4x10^5$ THP-1 cells were plated in a 24-well plate in RPMI Medium with 4.5 g/L glucose, 10 % heat inactivated fetal calf serum (Internegocios) and 2 mM L-glutamine (full medium) plus 50 nM phorbol 12-myristate 13-acetate (PMA) to allow differentiation of the cells to macrophages. On

the infection day, cells were washed and a suspension of the different strains of *M. tuberculosis* in RPMI medium was added. After 2 h of uptake, cells were washed 3 times with PBS and fresh full RPMI medium plus gentamicin 10 µg mL^{-1} was added. Cells were incubated at 37 °C in 5 % CO_2 atmosphere. Subsequently, at the indicated time points, cells were lysed in sterile water and serially diluted in PBS-Tween 80 0.05 %. Dilutions were plated on Middlebrook 7H10 complete agar medium (Difco Laboratories). Colonies were counted after 3 to 4 weeks to determine CFU.

Mouse infections

Bacillary suspensions of the different strains were adjusted to 100 viable cells in 100 ml phosphate buffer saline (PBS). Each animal was anesthetized and intratracheally inoculated with *M. tuberculosis* strains (*Mtb*H37Rv, *Mtb*Δ*fasR* and *Mtb*Δ*fasR*-c*fasR*). Infected mice were kept in cages fitted with microisolators connected to negative pressure. Groups of 10 mice were infected with the different *M. tuberculosis* strains. The inoculum doses were determined by enumerating CFU recovered from the lungs of three mice per strain, 24 h post-infection. Seven mice per group were killed at 60 days after infection and lungs removed and homogenized. Four dilutions of each homogenate were spread onto triplicate plates of Middlebrook 7H10 complete agar medium. The number of colonies was counted after 3 to 4 weeks.

Infection of THP-1 cells and indirect immunofluorescence (IFI)

522 *M. tuberculosis* strains were covalently stained with FITC (Sigma-Aldrich). Briefly,
523 1×10^9 bacteria were washed twice with 0.1 M PBS and suspended in 1 ml of the
524 same solution. FITC was added to a final concentration of 5 µg/ml and incubated in
525 the dark for 1 h at 37 °C. Bacteria were washed gently with PBS until
526 unincorporated dye was eliminated, and then were used to infect THP-1 cells.
527 THP-1 cells were maintained in complete full RPMI medium. The day before
528 infection $2x10^5$ THP-1 cells per well were plated in a 24-well plate with coverslips in
529 full RPMI medium plus 50 nM PMA to allow differentiation of the cells to
530 macrophages. On the day of infection, cells were washed and infected with the
531 different stained *M. tuberculosis* strains (*Mtb*H37Rv, *Mtb*Δ*fasR* and *Mtb*Δ*fasR*-
532 c*fasR*) prepared in RPMI medium, at a MOI of 5. After 2 h of uptake, cells were
533 washed and incubated with 10 µM Lysotracker Red DND-99 for 1 hour to allow the
534 staining of acidic compartments, fixed with 4 % paraformaldehyde solution in PBS
535 for 30 min and subjected to immunofluorescence analysis.
536 Cells were quenched by incubation with 50 mM NH_4Cl solution in PBS for 30 min.
537 and permeabilized with 0.05 % saponin/1 % BSA in PBS for 15 min, followed by
538 overnight incubation with goat anti-LAMP-3 (Santa Cruz Biotechnology, Santa
539 Cruz, CA) primary antibody diluted 1:50 in PBS. Secondary anti-goat antibody
540 conjugated to Cy3 (Jackson Immuno Research Labs, Inc.) was diluted 1:600 in
541 PBS. Cells were mounted with mounting medium (Dako, Denmark) and analysed
542 by confocal microscopy using an SP5 AOBS confocal microscope (Leica
543 Microsystems, Germany). Mycobacterial internalization was monitored by following
544 FITC fluorescence (green). Lysotracker Red DND-99 or LAMP-3 association with

mycobacterial phagosomes was analysed in at least 250 cells using Fiji software (U.S. National Institutes of Health, Bethesda, MD) as described previously (43). The experiments were performed in duplicates in three independent experiments. The statistical analysis was performed using two-tailed Student's t-test.

Acknowledgements

This research was supported by Agencia Nacional de Promoción de la Investigación, el Desarrollo Tecnológico y la Innovación (ANPCyT) grants 2011-0245, 2015-0796 and 2018-02539 to GG and 2015-2022 to HG and by National Institutes of Health grant 1R01AI095183-01 to HG. The funders had no role in study design, data collection and analysis, decision to publish, or preparation of the manuscript.

References

1. WHO. 2019. Global tuberculosis report.
2. Chiaradia L, Lefebvre C, Parra J, Marcoux J, Burlet-Schiltz O, Etienne G, Tropis M, Daffé M. 2017. Dissecting the mycobacterial cell envelope and defining the composition of the native mycomembrane. Sci Rep 7:12807.
3. Daffé M, Marrakchi H. 2019. Unraveling the Structure of the Mycobacterial Envelope. Microbiol Spectr 7:GPP3-0027–2018.
4. Brennan PJ, Nikaido H. 1995. The envelope of mycobacteria. AnnuRevBiochem 64:29–63.
5. Daffe M, Reyrat JM. 2008. The Mycobacterial Cell Envelope. ASM Press.
6. Russell DG, Barry CE, Flynn JL. 2010. Tuberculosis: What We Don't Know

Can, and Does, Hurt Us. Science 328:852–856.

7. Neyrolles O, Guilhot C. 2011. Recent advances in deciphering the contribution of Mycobacterium tuberculosis lipids to pathogenesis. Tuberculosis 91:187–195.

8. Passemar C, Arbues A, Malaga W, Mercier I, Moreau F, Lepourry L, Neyrolles O, Guilhot C, Astarie-Dequeker C. 2014. Multiple deletions in the polyketide synthase gene repertoire of mycobacterium tuberculosis reveal functional overlap of cell envelope lipids in host-pathogen interactions. Cell Microbiol 16:195–213.

9. Vromman F, Subtil A. 2014. Exploitation of host lipids by bacteria. Curr Opin Microbiol 17:38–45.

10. Teng O, En Ang CK, Guan XL. 2017. Macrophage-bacteria interactions-A lipid-centric relationship. Front Immunol 8.

11. Dulberger C, Rubin E, Boutte CC. 2020. The mycobacterial cell envelope — a moving target. Nat Rev Microbiol 18:47–59.

12. Mondino S, Gago G, Gramajo H. 2013. Transcriptional regulation of fatty acid biosynthesis in mycobacteria. Mol Microbiol 89:372–387.

13. Salzman V, Mondino S, Sala C, Cole ST, Gago G, Gramajo H. 2010. Transcriptional regulation of lipid homeostasis in mycobacteria. Mol Microbiol 78:64–77.

14. Boldrin F, Casonato S, Dainese E, Sala C, Dhar N, Palù G, Riccardi G, Cole ST, Manganelli R. 2010. Development of a repressible mycobacterial promoter system based on two transcriptional repressors. Nucleic Acids Res 38:1–11.

15. Cabruja M, Mondino S, Tsai YT, Lara J, Gramajo H, Gago G. 2017. A conditional mutant of the fatty acid synthase unveils unexpected cross talks in mycobacterial lipid metabolism. Open Biol 7.

16. Sassetti CM, Boyd DH, Rubin EJ. 2003. Genes required for mycobacterial growth defined by high density mutagenesis. MolMicrobiol 48:77–84.

17. Griffin JE, Gawronski JD, DeJesus MA, Ioerger TR, Akerley BJ, Sassetti CM. 2011. High-resolution phenotypic profiling defines genes essential for mycobacterial growth and cholesterol catabolism. PLoS Pathog 7:1–9.

18. DeJesus MA, Gerrick ER, Xu W, Park SW, Long JE, Boutte CC, Rubin EJ, Schnappinger D, Ehrt S, Fortune SM, Sassetti CM, Ioerger R. 2017. Comprehensive Essentiality Analysis of the Mycobacterium tuberculosis Genome via sturating transposon mutagenesis. MBio 8:e02133–1.

19. Zhu K, Zhang YM, Rock CO. 2009. Transcriptional regulation of membrane lipid homeostasis in Escherichia coli. JBiolChem 284:34880–34888.

20. Cuthbertson L, Nodwell JR. 2013. The TetR Family of Regulators. Microbiol Mol Biol Rev 77:440–475.

21. Fischer K, Chatterjee D, Torrelles J, Brennan PJ, Kaufmann SHE, Schaible UE. 2001. Mycobacterial Lysocardiolipin Is Exported from Phagosomes upon Cleavage of Cardiolipin by a Macrophage-Derived Lysosomal Phospholipase A 2 . J Immunol 167:2187–2192.

22. Graham JE, Clark-Curtiss JE. 1999. Identification of Mycobacterium tuberculosis RNAs synthesized in response to phagocytosis by human macrophages by selective capture of transcribed sequences (SCOTS). Proc Natl Acad Sci 96:11554–11559.

23. Rodríguez JE, Ramírez AS, Salas LP, Helguera-Repetto C, Gonzalez-y-Merchand J, Soto CY, Hernández-Pando R. 2013. Transcription of Genes Involved in Sulfolipid and Polyacyltrehalose Biosynthesis of Mycobacterium tuberculosis in Experimental Latent Tuberculosis Infection. PLoS One 8.

24. Griffin JE, Pandey AK, Gilmore SA, Mizrahi V, Mckinney JD, Bertozzi CR, Sassetti CM. 2012. Cholesterol catabolism by Mycobacterium tuberculosis requires transcriptional and metabolic adaptations. Chem Biol 19:218–227.

25. Yang X, Nesbitt NM, Dubnau E, Smith I, Sampson NS. 2009. Cholesterol Metabolism Increases the Metabolic Pool of Propionate in M. tuberculosis. Biochemistry 48:3819–3821.

26. Garcia-Vilanova A, Chan J, Torrelles JB. 2019. Underestimated Manipulative Roles of Mycobacterium tuberculosis Cell Envelope Glycolipids During Infection. Front Immunol 10.

27. Rohde K, Yates RM, Purdy GE, Russell DG. 2007. Mycobacterium tuberculosis and the environment within the phagosome. Immunol Rev 219:37–54.

28. Bah A, Sanicas M, Nigou J, Guilhot C, Astarie-Dequeker C, Vergne I. 2020. The Lipid Virulence Factors of Mycobacterium tuberculosis Exert Multilayered Control over Autophagy-Related Pathways in Infected Human Macrophages. Cells 9:666.

29. Cambier CJ., Takaki KK., Larson RP., Hernandez RE., Tobin DM., Urdahl KB., Cosma CL., Ramakrishnan L. 2014. Mycobacteria manipulate macrophage recruitment through coordinated use of membrane lipids. Nature 505:218–222.

30. Blanc L, Gilleron M, Prandi J, Song O, Jang M, Gicquel B, Drocourt D, Neyrolles O, Brodin P, Tiraby G, Vercellone A, Nigou J. 2017. Mycobacterium tuberculosis inhibits human innate immune responses via the production of TLR2 antagonist glycolipids. Proc Natl Acad Sci 114:11205–11210.

31. Camacho LR, Constant P, Raynaud C, Lane M, Triccas JA, Gicquel B, Daffe M, Guilhot C. 2001. Analysis of the Phthiocerol Dimycocerosate Locus of Mycobacterium tuberculosis. J Biol Chem 276:19845–19854.

32. Astarie-Dequeker C, Le Guyader L, Malaga W, Seaphanh FK, Chalut C, Lopez A, Guilhot C. 2009. Phthiocerol dimycocerosates of M. tuberculosis participate in macrophage invasion by inducing changes in the organization of plasma membrane lipids. PLoS Pathog 5:e1000289.

33. Rousseau C, Winter N, Pivert E, Bordat Y, Neyrolles O, Avé P, Huerre M, Gicquel B, Jackson M. 2004. Production of phthiocerol dimycocerosates protects Mycobacterium tuberculosis from the cidal activity of reactive nitrogen intermediates produced by macrophages and modulates the early immune response to infection. Cell Microbiol 6:277–287.

34. Lara J, Diacovich L, Trajtenberg F, Larrieux N, Malchiodi EL, Fernandez M, Gago G, Gramajo H, Buschiazzo A. 2020. Mycobacterium tuberculosis FasR senses long fatty acyl-CoA through a tunnel , inducing DNA-dissociation via a transmission spine. Nat Comm, in press.

35. Hanahan D. 1983. Studies on transformation of Escherichia coli with plasmids. JMolBiol 166:557–580.

36. Sambrook J. EFFTM. 1989. Molecular cloning: a laboratory manual, 2nd ed.

Cold Spring Harbor Laboratory Press, Cold Spring Harbor, N.Y.

37. Cole ST, Brosch R, Parkhill J, Garnier T, Churcher C, Harris D, Gordon S V, Eiglmeier K, Gas S, Barry III CE, Tekaia F, Badcock K, Basham D, Brown D, Chillingworth T, Connor R, Davies R, Devlin K, Feltwell T, Gentles S, Hamlin N, Holroyd S, Hornsby T, Jagels K, Krogh A, McLean J, Moule S, Murphy L, Oliver K, Osborne J, Quail MA, Rajandream MA, Rogers J, Rutter S, Seeger K, Skelton J, Squares R, Squares S, Sulston JE, Taylor K, Whitehead S, Barrell BG. 1998. Deciphering the biology of Mycobacterium tuberculosis from the complete genome sequence. Nature 393:537–544.

38. Connell ND. 1994. Mycobacterium: isolation, maintenance, transformation, and mutant selection. Methods Cell Biol 45:107–125.

39. Gomez JE, Bishai WR. 2000. whmD is an essential mycobacterial gene required for proper septation and cell division. Proc Natl Acad Sci U S A 97:8554–8559.

40. Muñoz-Elías EJ, McKinney JD. 2006. Carbon metabolism of intracellular bacteria. Cell Microbiol 8:10–22.

41. Kolly GS, Boldrin F, Sala C, Dhar N, Hartkoorn RC, Ventura M, Serafini A, Mckinney JD, Manganelli R, Cole ST. 2014. Assessing the essentiality of the decaprenyl-phospho-d-arabinofuranose pathway in Mycobacterium tuberculosis using conditional mutants. Mol Microbiol 92:194–211.

42. Layre E, Sweet L, Hong S, Madigan CA, Desjardins D, Young D, Cheng T, Annand JW, Kim K, Shamputa I, McConnell MJ, Debono CA, Behar SM, Minnaard AJ, Murray M, Barry III CE, Matsunaga I, Moody DB. 2011. A comparative lipidomics platform for chemotaxonomic analysis of

Mycobacterium tuberculosis. Chem Biol 23:1537–1549.

43. Vázquez CL, Bianco MV, Blanco FC, Forrellad MA, Gutierrez MG, Bigi F. 2017. Mycobacterium bovis Requires P27 (LprG) To Arrest Phagosome Maturation and Replicate within Bovine Macrophages. Infect Immun 85:1–11.

Figure legends

Fig 1. Schematic representation of the genetic organization of the chromosomal region of *fasR*.

(**A**) Wild type H37Rv strain (*Mtb*H37Rv), (**B**) *fasR* conditional knockdown strain (*Mtb*Δ*fasR*-c*fasR*) and (**C**) *fasR* KO strain (*Mtb*Δ*fasR*). (**D**) Southern Blot analysis of the different strains: chromosomal DNA was digested with *Xho*I and probed for hybridization with the probe indicated with a black bar, corresponding to the 5´ end of the *Rv3207* gene.

Fig 2. Growth of *M. tuberculosis* strains.

Growth curves of the wild type strain (*Mtb*H37Rv), the *fasR Mtb*Δ*fasR*-c*fasR* strain grown without ATc (complemented strain) and *fasR* KO strain (*Mtb*Δ*fasR*) were obtained in 3 different media (7H9 complete, 7H9 without OADC and Sauton). Growth was followed by measuring $OD_{600\ nm}$. Results are representative of three independent experiments.

Fig 3. Relative expression levels of *fasR*, *fas* and *acpS* mRNAs measured by quantitative RT-PCR.

Values were normalized to *sigA* and to the wild type strain (*Mtb*H37Rv). Samples for RNA extraction were collected at OD_{600nm} ~ 0.3.

Fig 4. Lipid profile in negative ion mode

LC-MS analyses (negative mode) of the phospholipids and mycolic acids present in the wild type strain (*Mtb*H37Rv), the *fasR* complemented strain (*Mtb*Δ*fasR*-c*fasR*) and *fasR* KO strain (*Mtb*Δ*fasR*). The values indicated represent the relative abundance of the MS signals corresponding to the different lipid classes found in the samples. Results are the means of three independent experiments. CL, cardiolipin; PI, phosphatidylinositol; PIM, phosphatidylinositol mannosides; PG, phosphatidylglycerol; PE, phosphatidylethanolamine; SL, sulfolipids; MA, mycolic acids.

Fig 5. Lipid profile in positive ion mode

LC-MS analyses (positive mode) of lipids present in the wild type strain (*Mtb*H37Rv), the *fasR* complemented strain (*Mtb*Δ*fasR*-c*fasR*) and *fasR* KO strain (*Mtb*Δ*fasR*). The values indicated represent the relative abundance of the MS signals corresponding to the different lipid classes found in the samples. Results are the means of three independent experiments. TAG, triacylglycerol; DAG, diacylglycerol; MMDAG, monomycolyl DAG; PDIM, phthiocerol dimycocerosates; GroMM, glycerol monomycolate; TMM, trehalose monomycolate.

736 **Fig 6. FasR is required for the intracellular survival of *M. tuberculosis*.**

737 THP-1-derived macrophages were infected with wild type *M. tuberculosis* H37Rv
738 (*Mtb*H37Rv), *fasR* mutant (*Mtb*Δ*fasR*) and the complemented *fasR* strain
739 (*Mtb*Δ*fasR*-c*fasR*) at a MOI =5. At different time post-infection (24, 48, 120, 144
740 hours) cells were washed and intracellular viable bacteria were counted on agar
741 plates. Bars represent the average of three independent experiments performed in
742 triplicate wells with standard deviation.

743

744 **Fig 7. FasR regulates phagosome maturation in macrophages.**

745 Confocal microscopy analysis of THP-1 macrophages infected with wild type *M.*
746 *tuberculosis* H37Rv (*Mtb*H37Rv), *fasR* mutant (*Mtb*Δ*fasR*) and the complemented
747 *fasR* strain (*Mtb*Δ*fasR*-*cfasR*). A) Representative images of THP-1 macrophages
748 infected with the different strains labelled with FITC (green fluorescence) using a
749 MOI=5. After 2 h of uptake, cells were washed and incubated with Lysotracker Red
750 DND-99 for 1 hour to allow the staining of acidic compartments, fixed and
751 subjected to immunofluorescence. The infected and fixed cells were used to detect
752 LAMP-3 by indirect immunofluorescence using a specific antibody against LAMP-3.
753 Scale bars: 10 μm. Merge indicates the location of the different strains in the
754 phagolysosome. B, C) Fluorescence intensity quantification of Lysotracker and
755 LAMP-3 associated with the phagosome of *M. tuberculosis Mtb*H37Rv (circles),
756 *Mtb*Δ*fasR* (squares) and the complemented *fasR* strain *Mtb*Δ*fasR*-*cfasR*
757 (triangles). Data were expressed in arbitrary units (a.u.). Fiji software was used for
758 quantification. Data represent means ± SEM of three independent experiments.

759 Asterisks indicate significance: *, P ≤ 0.05; **, P ≤ 0.01; and ***, P ≤ 0.001. Data
760 were analyzed using a two-tailed Student *t* test.
761
762 **Fig 8. FasR is essential for the multiplication of mycobacteria in mouse**
763 **lungs.**
764 Three groups of BALB/c mice (10 per group) were infected intratracheally with 10^2
765 CFU of *Mtb*H37Rv, *Mtb*Δ*fasR* and *Mtb*Δ*fasR*-c*fasR* strains and 60 days post-
766 infection bacterial loads in lungs were determined by plating serial dilutions on
767 Middlebrook 7H10 complete agar medium. The graph shows the mean values and
768 error bar of CFU. Data were analyzed using one-way ANOVA analysis and
769 Bonferroni's post-test. (**, P <0.01; ***, P ≤ 0.001).
770
771 **<u>Supplemental material</u>**
772
773 **Table S1.** Plasmids used in this study
774 **Table S2.** Strains used in this study
775 **Table S3.** Oligonucleotides used in this study
776 **Figure S1.** Analysis of the knockout fasR mutant (A) Colony PCR of M.
777 tuberculosis transformants grown on Str, carrying the complementing fasR gene
778 (clones 1 and 2) and of transformants grown on Hyg, carrying the empty pND255
779 vector (clones 3 and 4). Primers used for the amplification of fasR are listed in
780 Table S3. The expected size of the PCR products is 687 bp for the fasR wild type
781 allele and 150 bp for the mutant fasR allele. Two fragments were amplified from the
782 Str-resistant clones, corresponding to the complementing fasR gene from the

783 integrated plasmid and the deleted fasR gene at the fasR locus; on the other hand,
784 only one fragment was amplified from the Hyg resistant clones (the partially
785 deleted fasR gene) (B) Western Blot analysis of crude protein extracts prepared
786 from cultures of wild type H37Rv strain (MtbH37Rv), fasR conditional knockdown
787 strain (MtbΔfasR-cfasR) and fasR KO strain (MtbΔfasR clones 3 and 4) grown at
788 OD600nm ~ 0,3. Detection was performed using monoclonal anti-FasRMT
789 antibodies (lower panel) and anti-RpoB as loading control (upper panel).
790
791 **Figure S2.** Relative abundance of lipid species. The tables show the relative
792 abundance as the total signal percentage of the different lipid classes. CL,
793 cardiolipin; PE, phosphatidylethanolamine; PG, phosphatidylglycerol; PI,
794 phosphatidylinositol; PIMs, phosphatidylinositol mannosides; SL, sulfoglycolipids;
795 MA, mycolic acids; DAG, diacylglycerol; TAGs, triacylglycerol; MMDAG,
796 monomycolyl-DAG; GroMM, glycerol monomycolate; PDIM, phthiocerol
797 dimycocerosates; TMM, trehalose monomycolate. Results are the mean of three
798 independent experiments ± SD (n = 3). p values were calculated with unpaired t
799 test with Benjamini-Hochberg's correction between MtbΔfasR and MtbH37Rv.
800
801 **Figure S3.** Detailed analysis of lipid species. (A) The tables show the weighted
802 average of total number of carbons atoms per molecule within the population of
803 mycolic acids (MA), phospholipids (PE, phosphatidylethanolamine; CL, cardiolipin;
804 PG, phosphatidylglycerol; PI, phosphatidylinositol); sulfoglycolipids (SL); DAG,
805 diacylglycerol; GroMM, glycerol monomycolate; TAGs, triacylglycerol; TMM
806 trehalose monomycolate and phthiocerol dimycocerosates (PDIM A). The

807 histograms show the distribution of the number of carbon atoms of SL (B) and
808 PDIM (C) present in the wild type strain (MtbH37Rv), the fasR complemented
809 strain (MtbΔfasR-cfasR) and fasR mutant strain (MtbΔfasR). Results are the mean
810 of three independent experiments ± SD (n = 3). p values were calculated with
811 unpaired t test with Benjamini-Hochberg's correction between MtbΔfasR and
812 MtbH37Rv.
813
814 **Figure S4.** Saturation level of the fatty acid substituents of the phospholipids.
815 Histograms represent the levels of unsaturation of the fatty acids constituents of
816 cardiolipin (CL), phosphatidylglycerol (PG) and phosphatidylinositol (PI). Results
817 are the means of three independent experiments.

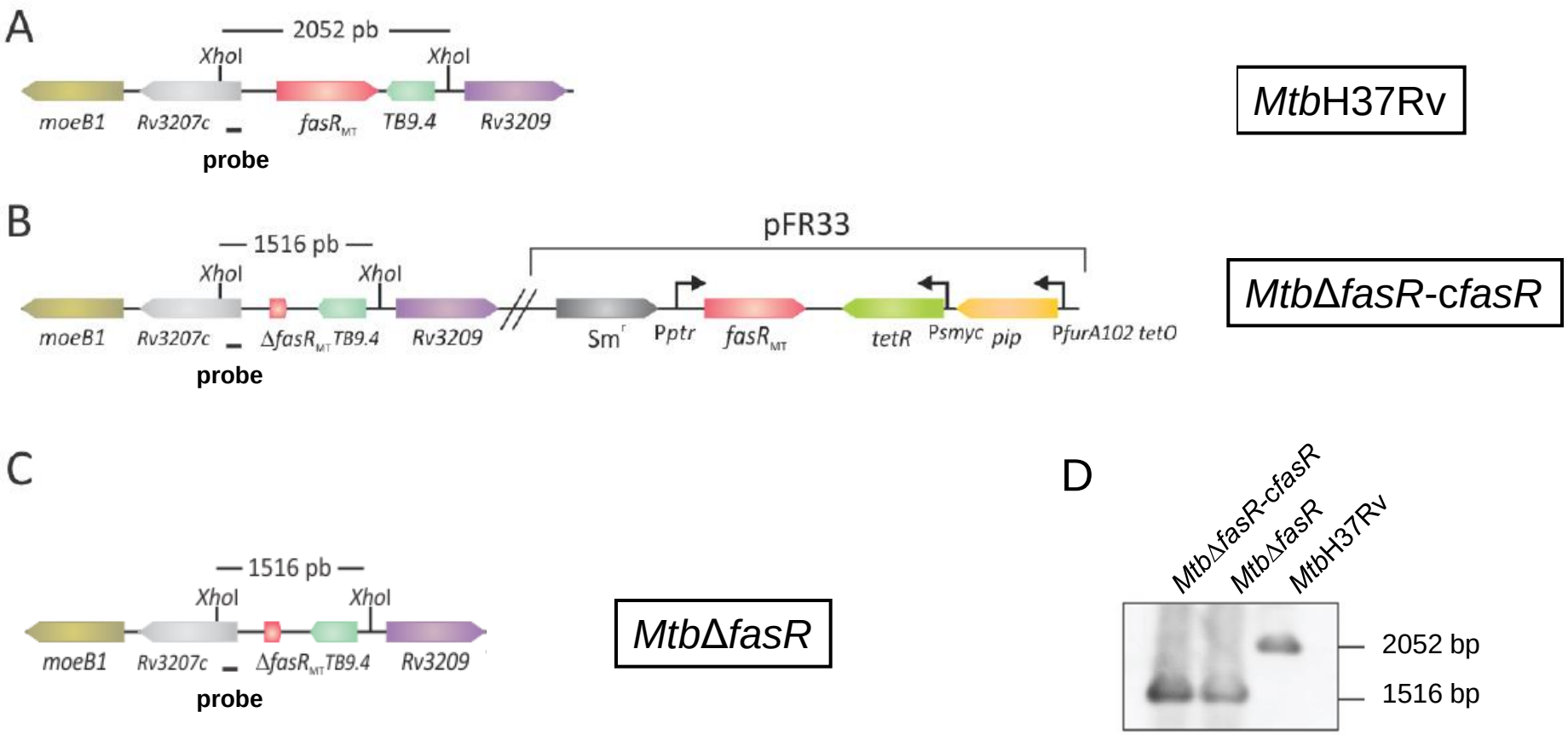

Fig 1. **Schematic representation of the genetic organization of the chromosomal region of *fasR.***
(**A**) Wild type H37Rv strain (*Mtb*H37Rv), (**B**) *fasR* conditional knockdown strain (*MtbΔfasR-cfasR*) and (**C**) *fasR* KO strain (*MtbΔfasR*). (**D**) Southern Blot analysis of the different strains: chromosomal DNA was digested with *Xho*I and probed for hybridization with the probe indicated with a black bar, corresponding to the 5´end of the *Rv3207* gene.

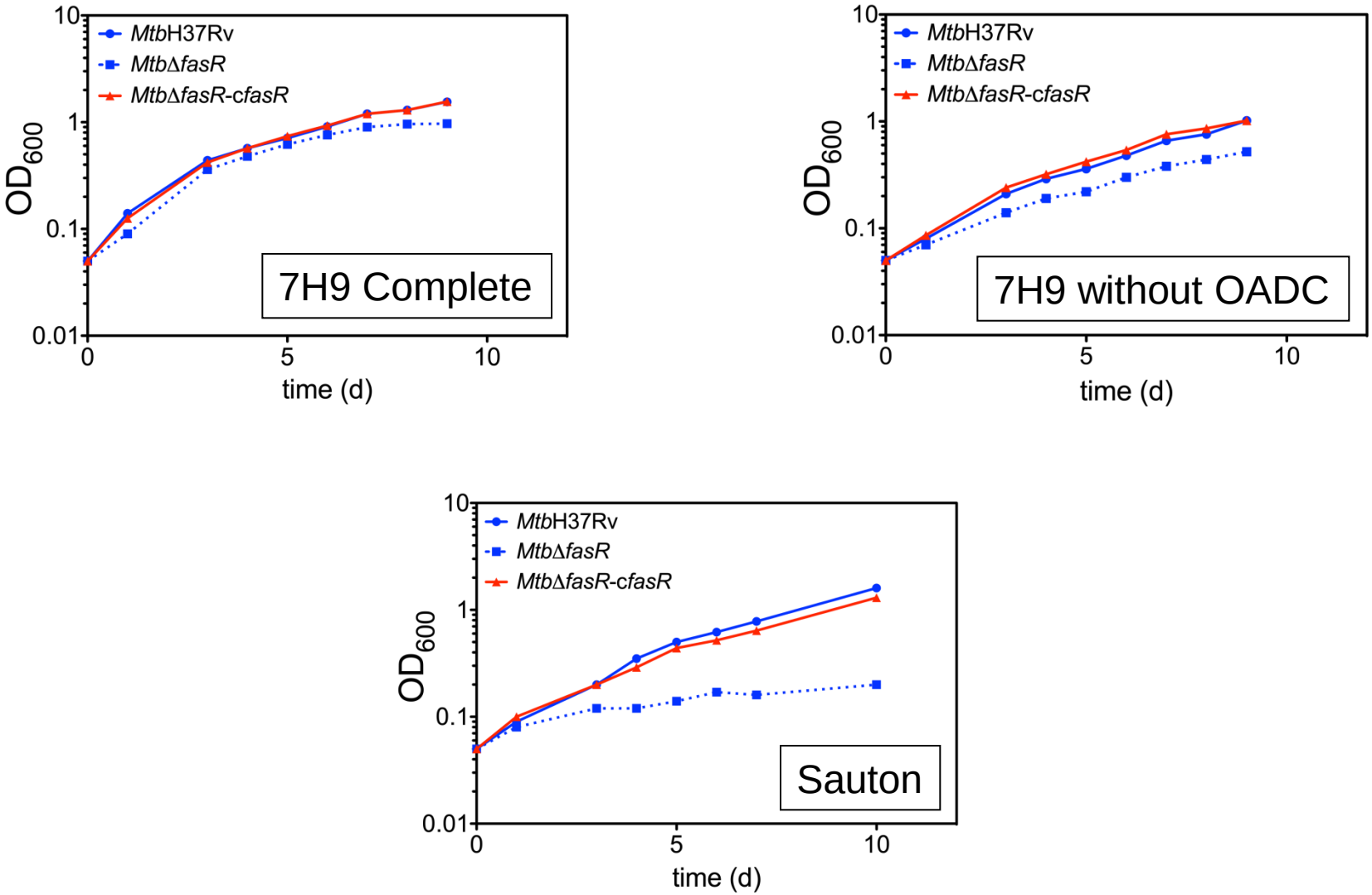

Fig 2. Growth of *M. tuberculosis* strains.
Growth curves of the wild type strain (*Mtb*H37Rv), the *fasR* *Mtb*Δ*fasR*-c*fasR* strain grown without ATc (complemented strain) and *fasR* KO strain (*Mtb*Δ*fasR*) were obtained in 3 different media (7H9 complete, 7H9 without OADC and Sauton). Growth was followed by measuring $OD_{600\ nm}$. Results are representative of three independent experiments.

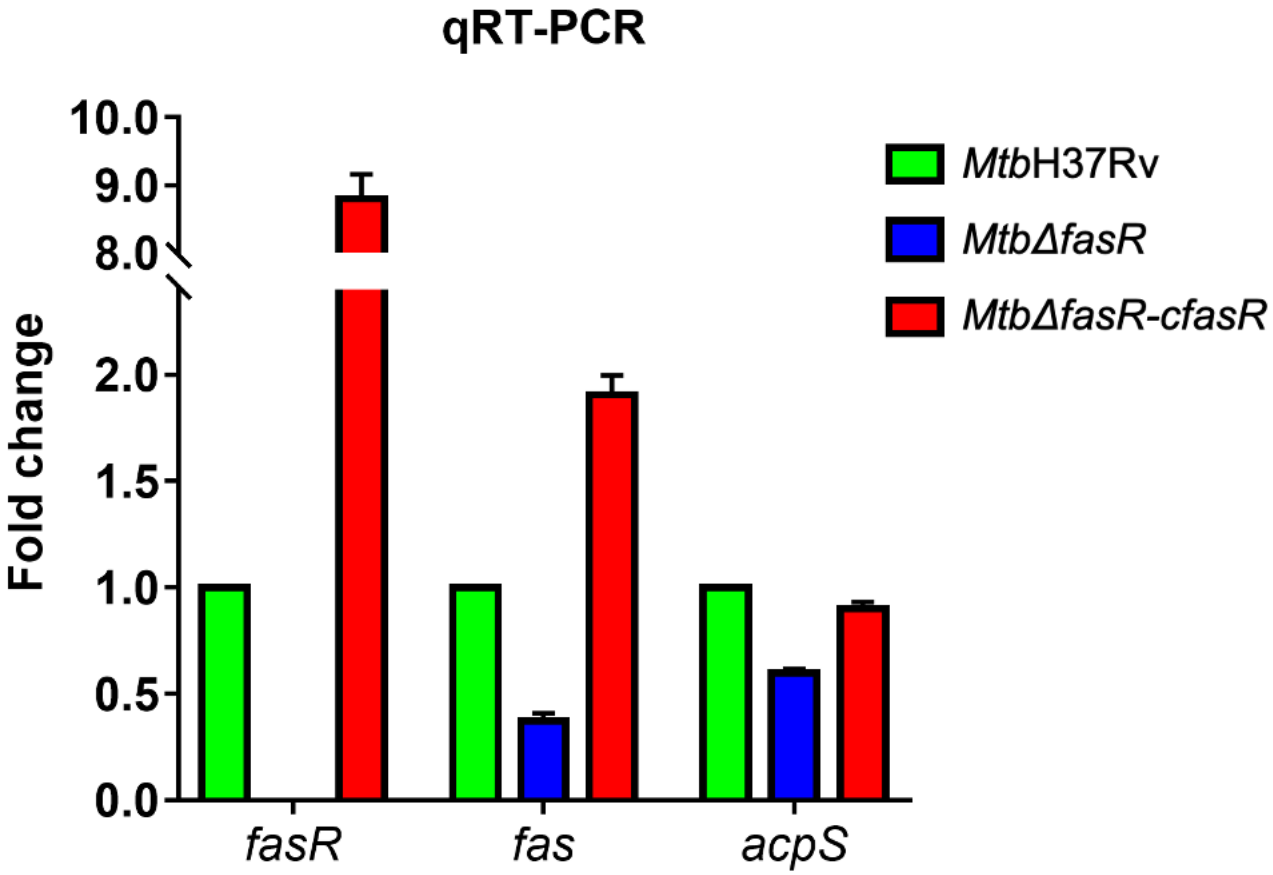

Fig 3. Relative expression levels of *fasR*, *fas* and *acpS* mRNAs measured by quantitative RT-PCR.
Values were normalized to *sigA* and to the wild type strain (*Mtb*H37Rv). Samples for RNA extraction were collected at OD_{600nm} ~ 0,3.

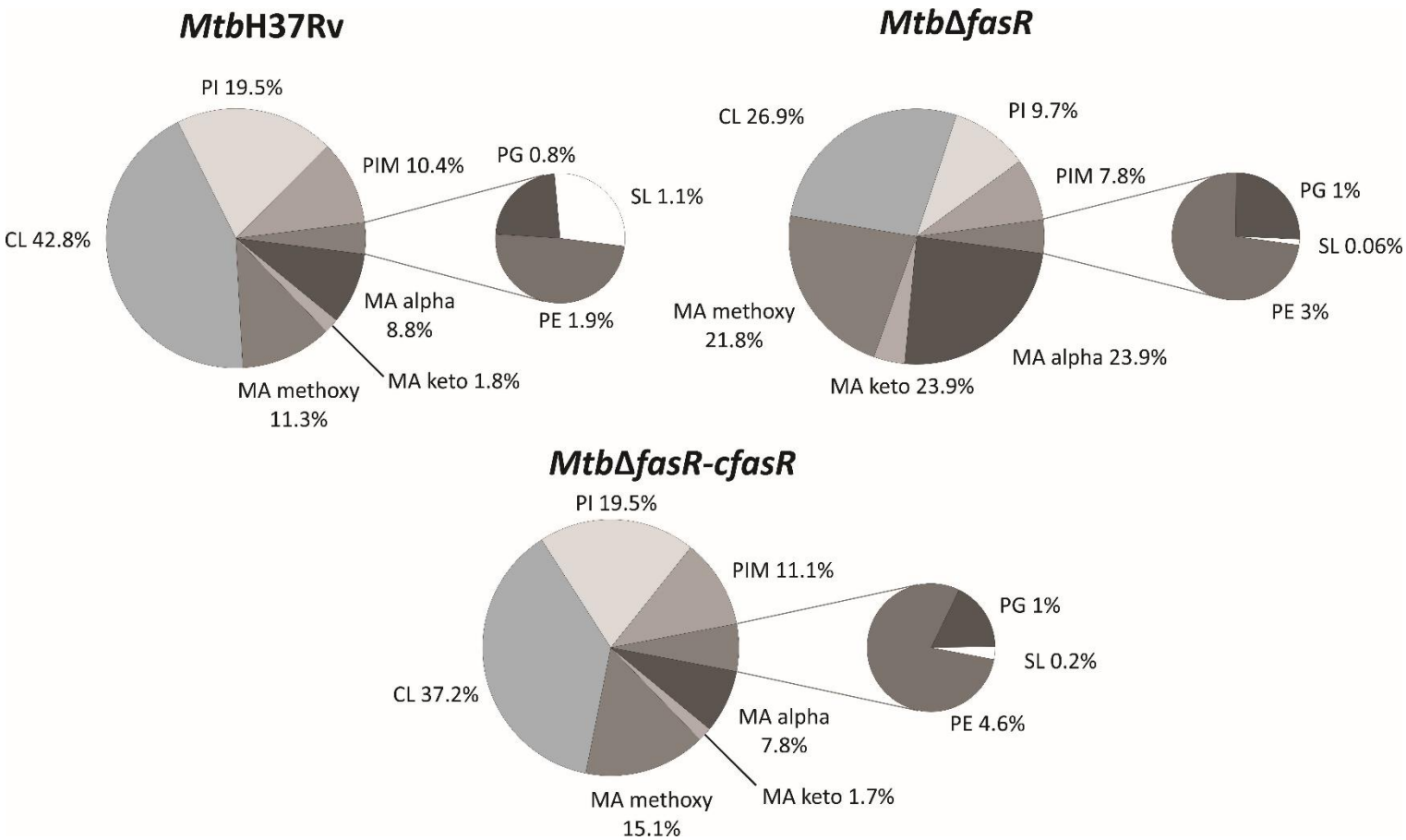

Mycolic acids		Phospholipids	
*Mtb*H37Rv	25%	*Mtb*H37Rv	75%
*Mtb*Δ*fasR*	50%	*Mtb*Δ*fasR*	50%
*Mtb*Δ*fasR-cfasR*	22%	*Mtb*Δ*fasR-cfasR*	78%

Fig 4. Lipid profile in negative ion mode

LC-MS analyses (negative mode) of the phospholipids and mycolic acids present in the wild type strain (*Mtb*H37Rv), the *fasR* complemented strain (*Mtb*Δ*fasR*-c*fasR*) and *fasR* KO strain (*Mtb*Δ*fasR*). The values indicated represent the relative abundance of the MS signals corresponding to the different lipid classes found in the samples. Results are the means of three independent experiments. CL, cardiolipin; PI, phosphatidylinositol; PIM, phosphatidylinositol mannosides; PG, phosphatidylglycerol; PE, phosphatidylethanolamine; SL, sulfolipids; MA, mycolic acids.

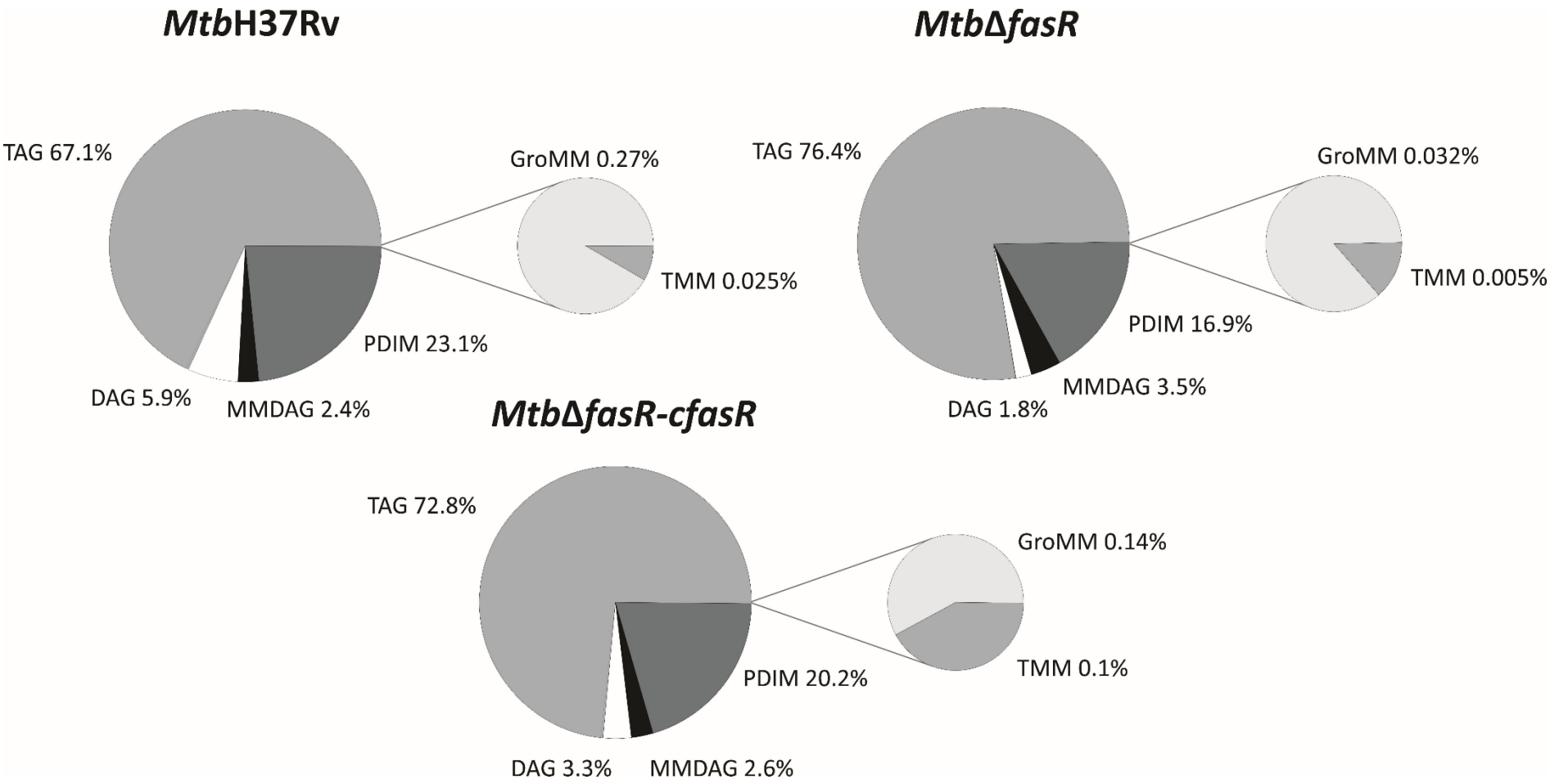

Fig 5. Lipid profile in positive ion mode

LC-MS analyses (positive mode) of lipids present in the wild type strain (*Mtb*H37Rv), the *fasR* complemented strain (*Mtb*Δ*fasR*-c*fasR*) and *fasR* KO strain (*Mtb*Δ*fasR*). The values indicated represent the relative abundance of the MS signals corresponding to the different lipid classes found in the samples. Results are the means of three independent experiments. TAG, triacylglycerol; DAG, diacylglycerol; MMDAG, monomycolyl DAG; PDIM, phthiocerol dimycocerosates; GroMM, glycerol monomycolate; TMM, trehalose monomycolate.

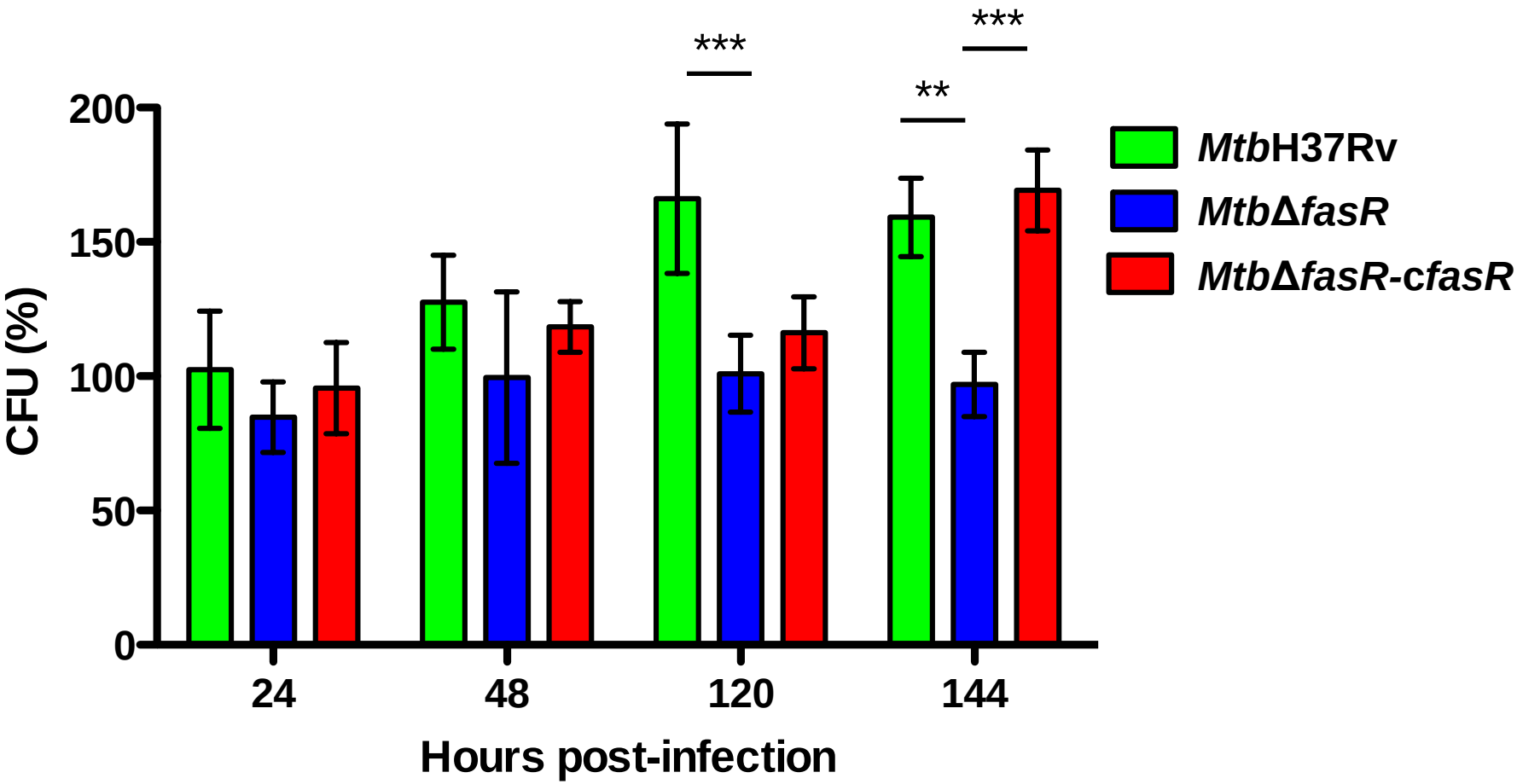

Fig 6. FasR is required for the intracellular survival of *M. tuberculosis*.
THP-1-derived macrophages were infected with wild type *M. tuberculosis* H37Rv (*Mtb*H37Rv), *fasR* mutant (*Mtb*Δ*fasR*) and the complemented *fasR* strain (*Mtb*Δ*fasR*-c*fasR*) at a MOI =5. At different time post-infection (24, 48, 120, 144 hours) cells were washed and intracellular viable bacteria were counted on agar plates. Bars represent the average of three independent experiments performed in triplicate wells with standard deviation.

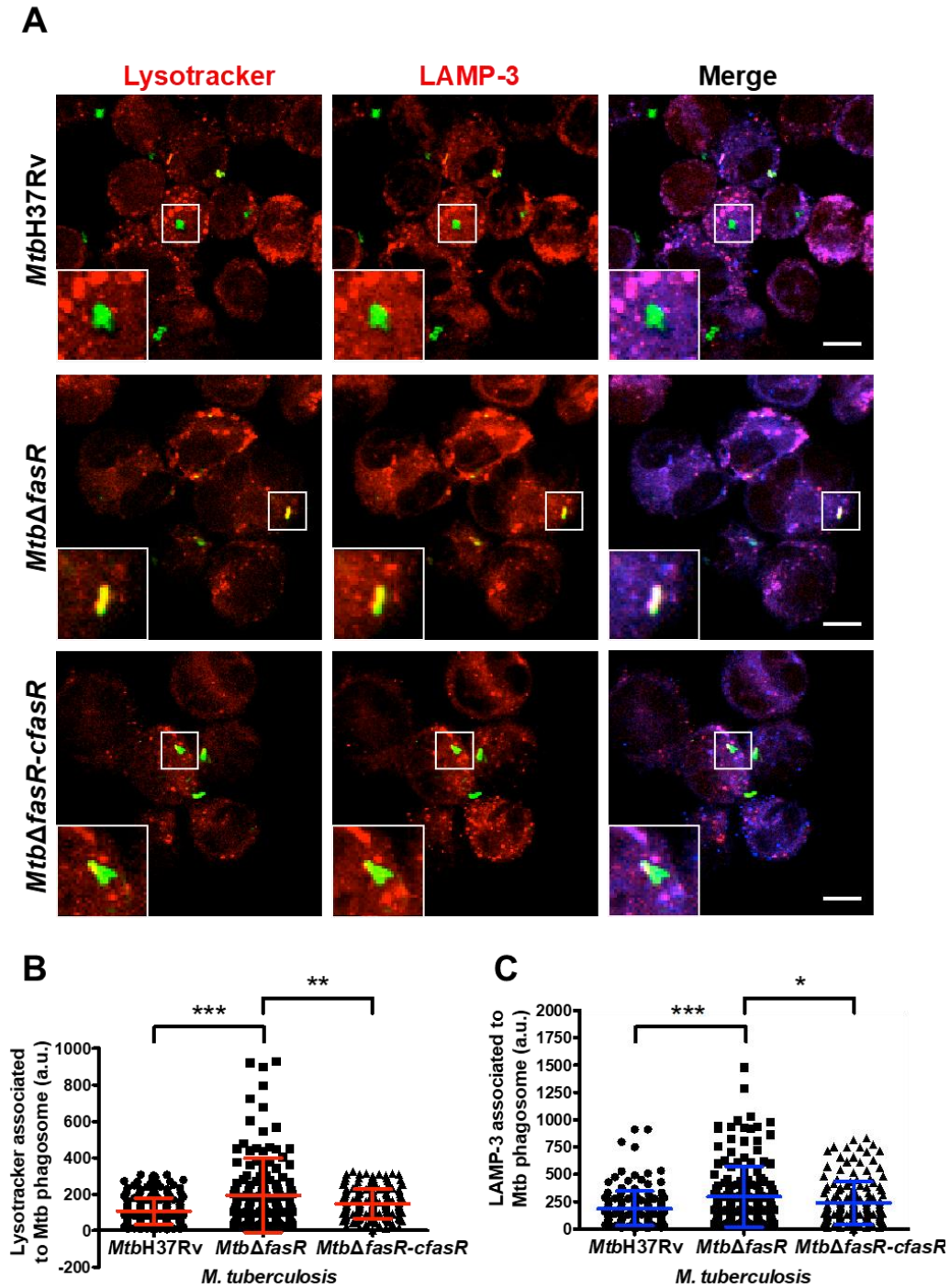
A
Lysotracker
LAMP-3
Merge
MtbH37Rv
MtbΔfasR
MtbΔfasR-cfasR
B
Lysotracker associated to Mtb phagosome (a.u.)
1000
800
600
400
200
0
-200
***
**
MtbH37Rv
MtbΔfasR
MtbΔfasR-cfasR
M. tuberculosis
C
LAMP-3 associated to Mtb phagosome (a.u.)
2000
1750
1500
1250
1000
750
500
250
0
***
*
MtbH37Rv
MtbΔfasR
MtbΔfasR-cfasR
M. tuberculosis

Fig 7. FasR regulates phagosome maturation in macrophages.

Confocal microscopy analysis of THP-1 macrophages infected with wild type *M. tuberculosis* H37Rv (*Mtb*H37Rv), *fasR* mutant (*Mtb*Δ*fasR*) and the complemented *fasR* strain (*Mtb*Δ*fasR-cfasR*). A) Representative images of THP-1 macrophages infected with the different strains labelled with FITC (green fluorescence) using a MOI=5. After 2 h of uptake, cells were washed and incubated with Lysotracker Red DND-99 for 1 hour to allow the staining of acidic compartments, fixed and subjected to immunofluorescence. The infected and fixed cells were used to detect LAMP-3 by indirect immunofluorescence using a specific antibody against LAMP-3. Scale bars: 10 μm. Merge indicates the location of the different strains in the phagolysosome. B, C) Fluorescence intensity quantification of Lysotracker and LAMP-3 associated with the phagosome of *M. tuberculosis Mtb*H37Rv (circles), *Mtb*Δ*fasR* (squares) and the complemented *fasR* strain *Mtb*Δ*fasR-cfasR* (triangles). The data were expressed in arbitrary units (a.u.). Fiji software was used for quantification. Data represent the means ±the SEM of three independent experiments. The asterisks indicate significance: *, $P \leq 0.05$; **, $P \leq 0.01$; and ***, $P \leq 0.001$. The data were analyzed using a two-tailed Student *t* test.

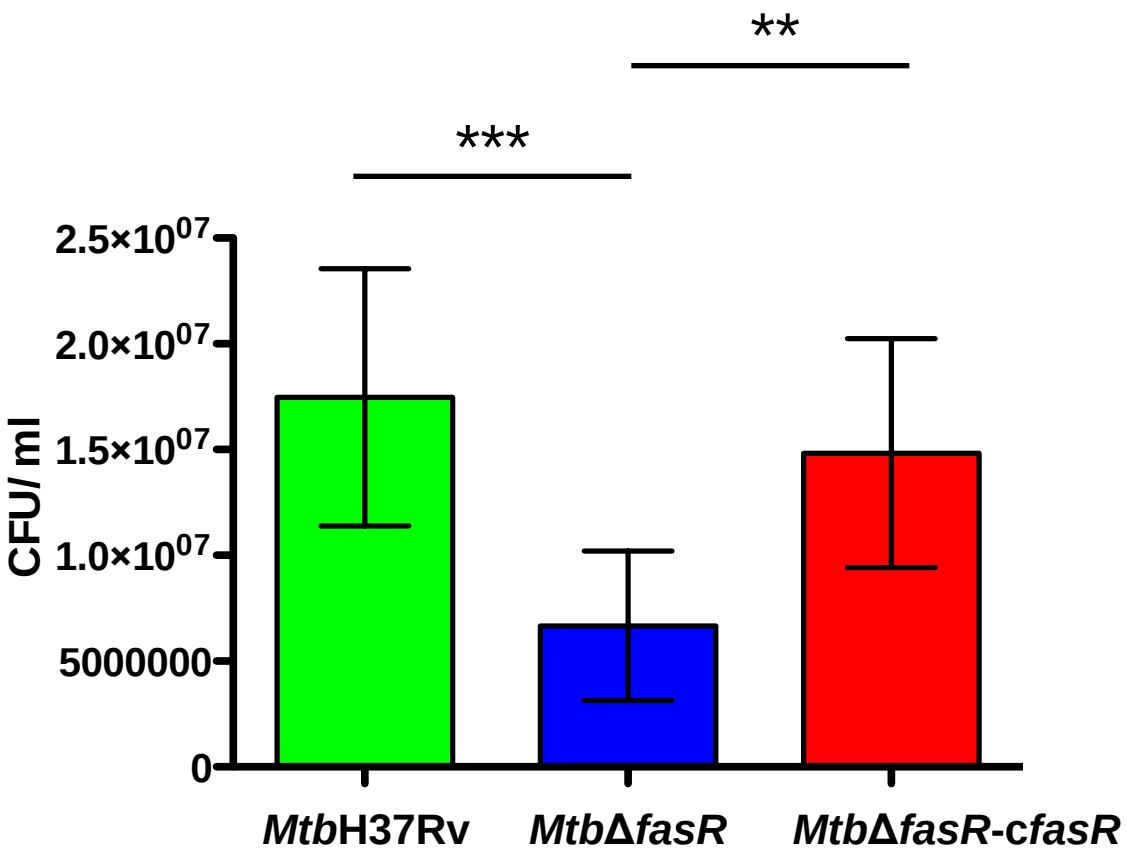

Fig 8. FasR is essential for the multiplication of mycobacteria in mouse lungs.
Three groups of BALB/c mice (10 per group) were infected intratracheally with 10^2 CFU of *Mtb*H37Rv, *Mtb*Δ*fasR* and *Mtb*Δ*fasR*-c*fasR* strains and 60 days post-infection bacterial loads in lungs were determined by plating serial dilutions on Middlebrook 7H10 complete agar medium. The graph shows the mean values and error bar of CFU. Data were analyzed using one-way ANOVA analysis and Bonferroni's post-test. (**, P <0.01; ***, P ≤ 0.001).

Table S1. Plasmids used in this study

Name	Description and features	References
pFR3	pET28a(+) with *fasR* His tag fusion gene, under the control of T7 promoter, Kan^R	(1)
pJG1100	Suicide vector for mutant construction, Hyg^R, Kan^R, *sacB*	(2)
pFR35	Suicide vector for *Mtb*Δ*fasR* mutant construction derived from pJG1100, Hyg^R, Kan^R, *sacB*	This study
pGA44	Integrative vector at L5 *attB* site, carrying the TetR/Pip OFF expression system and Ptr promoter, Str^R/$Spect^R$ The *int* gene was removed in order to lock this plasmid at the integration site. Integration requires plasmid pGA80	(3)
pGA80	pMV261-derived vector, carrying the L5 *int* gene for expression in *trans*, lacking the mycobacterial origin of replication (Δ*oriM*), Kan^R	(3)
pFR33	pGA44-derived vector carrying *fasR* under the control of the Ptr promoter, Str^R/$Spect^R$	This study
pND255	L5-integrative vector for mutant construction, Hyg^R	(3)

Hyg^R, hygromicin resistance; Kan^R, kanamycin resistance; Str^R/$Spect^R$, streptomycin/spectinomycin resistance

Table S2. Strains used in this study

Name	Description or Genotype	References
DH5α	*E. coli K12 F- ΔlacU169 (ϕ80lacZΔM15) endA1 recA1 hsdR17 deoR supE44 thi-1λ-gyrA96 relA1*	(4)
*Mtb*H37Rv	*M. tuberculosis* wild type strain	(5)
*Mtb*Δ*fasR*	*Mtb*H37Rv background. Deletion of *fasR*	This study
*Mtb*Δ*fasR-cfasR*	*fasR* knockout complemented with *fasR* expressed *in trans*	This study

Table S3. Oligonucleotides used in this study

Name	Sequence (5'-3')
3208_1up	CTCGAGCCGGAATTCGTAGCC
3208_2down	CATATGGAGCGCTGCCGGACGATCTG
3208_3up	CATATGAAGCCGATTTCCAAGTCCGAC

3208_4down	ACTAGTTGCCACCGTGGTGACCGTCTC
Southern_1fasRTB	GAACACTTTGACGGTGCCTTG
Southern_2fasRTB	GGAATGACATTACTACCTGCG
L-*sigA*	AAACAGATCGGCAAGGTAGC
R-*sigA*	CTGGATCAGGTCGAGAAACG
L-*fasR*	TGAGCACGACTACCGACAAC
R-*fasR*	CTCGAAGATCAGCCGGTAAC
L-*fas*	GACATCCTGACCCGACTGAC
R-*fas*	TGAACTTCGTCGAGAGCTTG
fasRF	ATGAGCGATCTCGCCAAGACAG
fasRR	CTACGAGCGGGTAAGCGGGACG

References

1. Mondino S, Gago G, Gramajo H. 2013. Transcriptional regulation of fatty acid biosynthesis in mycobacteria. Mol Microbiol 89:372–387.
2. Gomez JE, Bishai WR. 2000. whmD is an essential mycobacterial gene required for proper septation and cell division. Proc Natl Acad Sci U S A 97:8554–8559.
3. Kolly GS, Boldrin F, Sala C, Dhar N, Hartkoorn RC, Ventura M, Serafini A, Mckinney JD, Manganelli R, Cole ST. 2014. Assessing the essentiality of the decaprenyl-phospho-d-arabinofuranose pathway in Mycobacterium tuberculosis using conditional mutants. Mol Microbiol 92:194–211.
4. Hanahan D. 1983. Studies on transformation of Escherichia coli with plasmids. JMolBiol 166:557–580.
5. Cole ST, Brosch R, Parkhill J, Garnier T, Churcher C, Harris D, Gordon S V, Eiglmeier K, Gas S, Barry III CE, Tekaia F, Badcock K, Basham D, Brown D, Chillingworth T, Connor R, Davies R, Devlin K, Feltwell T, Gentles S, Hamlin N, Holroyd S, Hornsby T, Jagels K, Krogh A, McLean J, Moule S, Murphy L, Oliver K, Osborne J, Quail MA, Rajandream MA, Rogers J, Rutter S, Seeger K, Skelton J, Squares R, Squares S, Sulston JE, Taylor K, Whitehead S, Barrell BG. 1998. Deciphering the biology of Mycobacterium tuberculosis from the complete genome sequence. Nature 393:537–544.

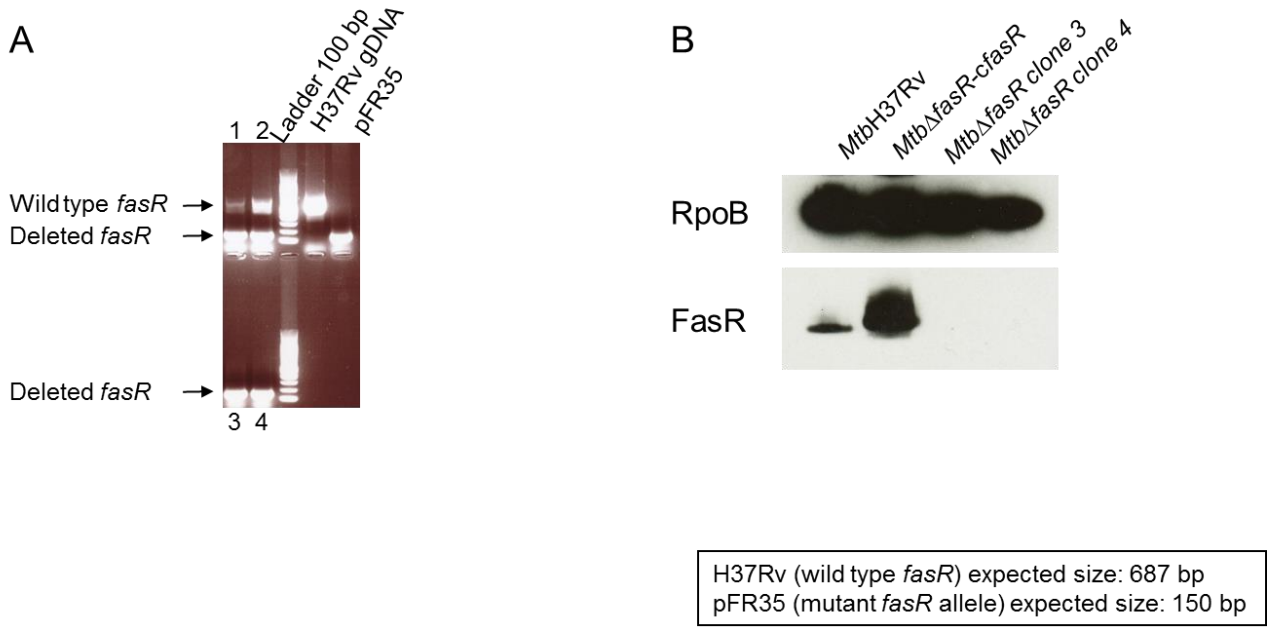

Figure S1. Analysis of the knockout *fasR* mutant (A) Colony PCR of *M. tuberculosis* transformants grown on Str, carrying the complementing *fasR* gene (clones 1 and 2) and of transformants grown on Hyg, carrying the empty pND255 vector (clones 3 and 4). Primers used for the amplification of *fasR* are listed in Table S3. The expected size of the PCR products is 687 bp for the *fasR* wild type allele and 150 bp for the mutant *fasR* allele. Two fragments were amplified from the Str-resistant clones, corresponding to the complementing *fasR* gene from the integrated plasmid and the deleted *fasR* gene at the *fasR* locus; on the other hand, only one fragment was amplified from the Hyg resistant clones (the partially deleted *fasR* gene) **(B)** Western Blot analysis of crude protein extracts prepared from cultures of wild type H37Rv strain (*Mtb*H37Rv), *fasR* conditional knockdown strain (*Mtb*Δ*fasR*-c*fasR*) and *fasR* KO strain (*Mtb*Δ*fasR* clones 3 and 4) grown at OD_{600nm} ~ 0,3. Detection was performed using monoclonal anti-$FasR_{MT}$ antibodies (lower panel) and anti-RpoB as loading control (upper panel).

Lipid profile in negative ion mode: signal %				
	*MtbH*37Rv	*MtbΔfasR*	*MtbΔfasR-cfasR*	*p-value**
CL	36.37 ± 2.43	20.87 ± 3.34	31.52 ± 0.78	0.0234
PE	1.54 ± 1.43	2.31 ± 1.25	3.92 ± 1.23	0.624
PG	0.74 ± 0.11	0.82 ± 0.07	0.86 ± 0.25	0.4725
PI	16.71 ± 2.26	7.49 ± 0.09	16.45 ± 3.35	0.0234
PIMs	8.97 ± 2.43	6.01 ± 1.06	9.35 ± 2.74	0.1851429
MA alpha	7.54 ± 1.43	18.44 ± 0.61	6.7 ± 2.2	0.018
MA keto	1.54 ± 0.22	2.98 ± 0.42	1.5 ± 0.62	0.0234
MA methoxy	9.66 ± 2.3	16.78 ± 0.22	13 ± 8.58	0.03825
SL	0.89 ± 0.71	0.04 ± 0.03	0.16 ± 0.04	0.0234

* T-test *MtbΔfasR vs MtbH*37Rv. Benjamini-Hochberg adjusted *p-value*.

Lipid profile in positive ion mode: signal %				
	*MtbH*37Rv	*MtbΔfasR*	*MtbΔfasR-cfasR*	*p-value**
DAG	5.91 ± 1.37	1.84 ± 1.28	3.29 ± 0.19	0.0538
TAGs	67.15 ± 2.5	76.39 ± 0.61	72.78 ± 4.64	0.0246
MMDAG	2.43 ± 0.19	3.54 ± 0.25	2.57 ± 0.12	0.0246
GroMM	0.27 ± 0.13	0.03 ± 0.01	0.14 ± 0.047	0.0898
PDIM	23.1 ± 1.56	16.94 ± 0.24	20.22 ± 4.39	0.0246
TMM	0.02 ± 0.004	0.005 ± 0.001	0.1 ± 0.01	0.0246

* T-test *MtbΔfasR vs MtbH*37Rv. Benjamini-Hochberg adjusted *p-value*.

Figure S2. Relative abundance of lipid species. The tables show the relative abundance as the total signal percentage of the different lipid classes. CL, cardiolipin; PE, phosphatidylethanolamine; PG, phosphatidylglycerol; PI, phosphatidylinositol; PIMs, phosphatidylinositol mannosides; SL, sulfoglycolipids; MA, mycolic acids; DAG, diacylglycerol; TAGs, triacylglycerol; MMDAG, monomycolyl-DAG; GroMM, glycerol monomycolate; PDIM, phthiocerol dimycocerosates; TMM, trehalose monomycolate. Results are the mean of three independent experiments ± SD (n = 3). p values were calculated with unpaired *t* test with Benjamini-Hochberg's correction between *MtbΔfasR* and *Mtb*H37Rv.

A)

Lipid profile in negative ion mode: C – chain length				
	*MtbH*37Rv	*MtbΔfasR*	*MtbΔfasR-cfasR*	*p-value**
CL	68.71 ±0.02	68.65 ±0.14	68.95 ±0.05	0.017
PE	34.4 ±0.28	34.32 ±0.08	34.33 ±0.21	0.909
PG	34.2 ±0.11	34.17 ±0.17	34.3 ±0.03	0.219
PI	34.93 ±0.04	34.96 ±0.12	34.99 ±0.04	0.711
MA alpha	78.64 ±0.004	78.37 ±0.04	78.52 ±0.09	0.078
MA keto	84.64 ±0.03	83.65 ±0.28	84.3 ±0.08	0.016
MA methoxy	85.34 ±0.34	84.77 ±0.02	85.12 ±0.05	0.002
SL	151.04 ±0.27	144.01 ±1.61	148.84 ±0.72	0.013
Lipid profile in positive ion mode: C – chain length				
	*MtbH*37Rv	*MtbΔfasR*	*MtbΔfasR-cfasR*	*p-value**
DAG	35.49 ±0.09	36.82 ±0.96	35.28 ±0.06	0.031
GroMM	47.61 ±0.15	46.67 ±0.9	46.49 ±0.93	0.018
TAGs	55.87 ±0.21	58.65 ±0.43	56.34 ±0.33	0.003
TMM alpha	82.16 ±0.13	81.22 ±0.13	80.89 ±0.4	0.237
TMM keto	87.07 ±0.13	86.07 ±0.65	86.69 ±0.15	0.106
TMM methoxy	87.51 ±0.12	86.39 ±0.31	87.32 ±0.47	0.052
PDIM A	93.19 ±0.26	91.17 ±0.21	92.65 ±0.03	0.0005

* T-test *MtbΔfasR vs MtbH*37Rv. Benjamini-Hochberg adjusted *p-value*.

B)

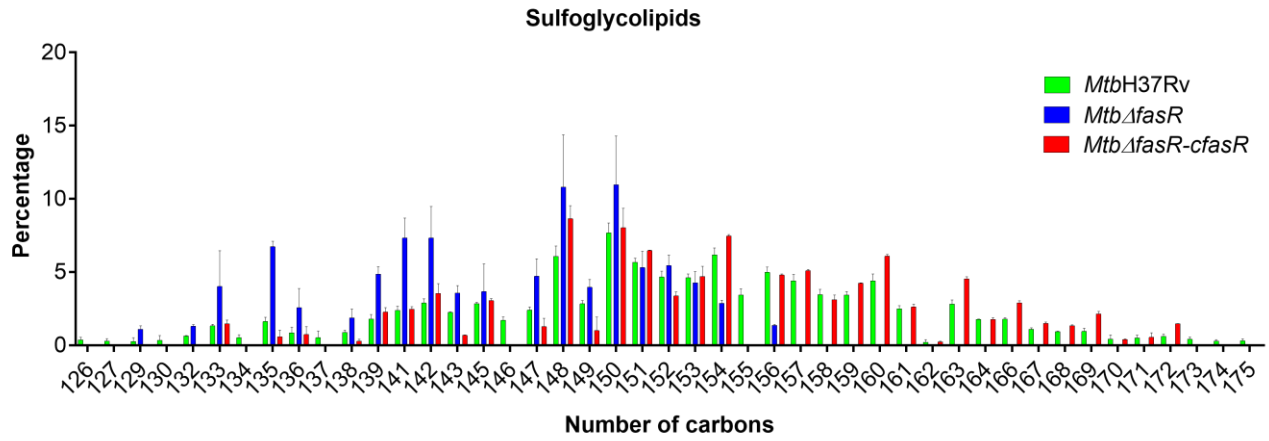

C)

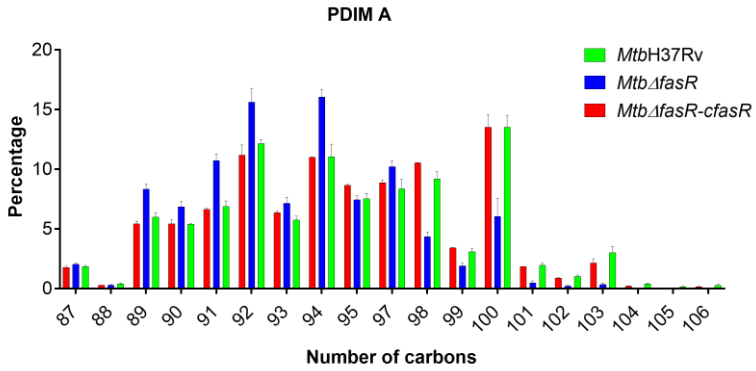

Figure S3. Detailed analysis of lipid species. (A) The tables show the weighted average of total number of carbons atoms per molecule within the population of mycolic acids (MA), phospholipids (PE, phosphatidylethanolamine; CL, cardiolipin; PG, phosphatidylglycerol; PI, phosphatidylinositol); sulfoglycolipids (SL); DAG, diacylglycerol; GroMM, glycerol monomycolate; TAGs, triacylglycerol; TMM trehalose monomycolate and phthiocerol dimycocerosates (PDIM A). The histograms show the distribution of the number of carbon atoms of SL **(B)** and PDIM **(C)** present in the wild type strain (*Mtb*H37Rv), the *fasR* complemented strain (*Mtb*Δ*fasR*-c*fasR*) and *fasR* mutant strain (*Mtb*Δ*fasR*). Results are the mean of three independent experiments ± SD (n = 3). p values were calculated with unpaired *t* test with Benjamini-Hochberg's correction between *Mtb*Δ*fasR* and *Mtb*H37Rv.

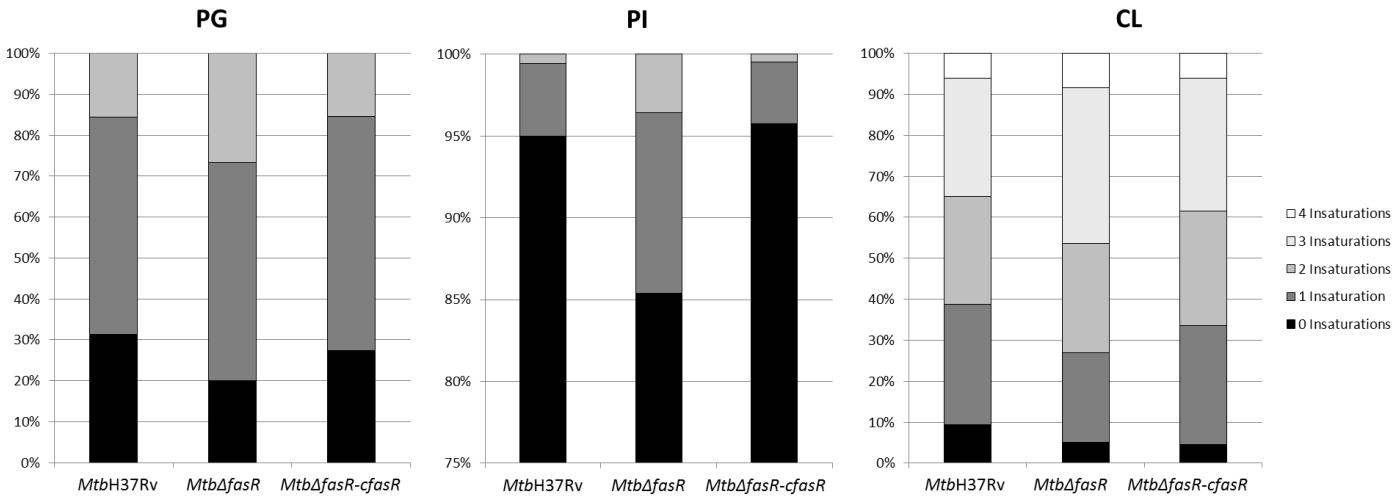

Figure S4. Saturation level of the fatty acid substituents of the phospholipids. Histograms represent the levels of unsaturation of the fatty acids constituents of cardiolipin (CL), phosphatidylglycerol (PG) and phosphatidylinositol (PI). Results are the means of three independent experiments.